A NEW APPROACH IN BLADE SHAPE ADJUSTMENT IN PBD-14 DESIGN MODE

by

ARISTOMENIS CHRISOSPATHIS

B.S., Marine Engineering (1992)

Hellenic Naval Academy

Submitted to the Department of Ocean Engineering

in Partial Fulfillment of the Requirements for the Degrees of

Naval Engineering and

Master of Science in Ocean Systems Management

at the

Massachusetts Institute of Technology

June 2001

Signature of Author..... .....

Department of Ocean Engineering

May 11, 2001

Certified by..... .....

Justin E. Kerwin, Professor of Naval Architecture

Thesis Supervisor, Department of Ocean Engineering

Certified by..... .....

Henry S. Marcus, Professor of Marine Systems

Thesis Reader, Department of Ocean Engineering

Accepted by..... .....

Henrik Schmidt, Professor of Ocean Engineering

Chairman, Department Committee on Graduate Students

A NEW APPROACH IN BLADE SHAPE ADJUSTMENT IN PBD-14 DESIGN MODE

by
Aristomenis Chrisospathis

Submitted to the Department of Ocean Engineering on May 11, 2001, for the partial fulfillment of the requirements for the Degrees of
Naval Engineering and
Master of Science in Ocean Systems Management.

Abstract

The purpose of this study is to develop a more efficient and robust algorithm for adjusting the blade shape as a part of a coupled lifting-surface design/analysis code for marine propulsors developed at MIT, known as *PBD-14*. The algorithm for adjusting the blade shape in the current version of *PBD-14* works satisfactorily in most cases. However, with more complex schemes such as ducted propulsors and/or higher load distributions, the process has to be carefully monitored by the user and the blade surface can develop corrugations in the spanwise direction.

A different approach investigated in this study is based on an idea of aligning the blade shape by tracing streamlines. In order to satisfy the kinematic boundary condition, the final blade shape has to exactly match the streamlines of the flow field in which the propeller blade operates. The algorithm that is developed traces streamlines by calculating the total velocity on a grid of points and then exactly fits the blade on this grid of points. Initial tests of this algorithm have demonstrated its robustness by producing accurate blade shapes both in uniform and in more complicated flow fields.

Finally, propeller fabrication is investigated, and tolerance issues as well as propeller inspection methods, traditional and modern, are examined. A cost analysis is performed that investigates the economic impact of manufacturing an example propeller according to a certain tolerance system.

Thesis Supervisor: Justin E. Kerwin

Title: Professor of Naval Architecture

ACKNOWLEDGMENTS

This thesis would have never been accomplished without the valuable love and the continuous support, throughout my whole education, of my beloved parents, Dimitri and Eleni, to who I wish to dedicate it. I also wish to express my deepest gratitude to all my good friends who supported me throughout my graduate studies in many ways.

I wish to thank my thesis advisor, Professor Jake Kerwin, for his guidance and support throughout the last year. I would also like to thank Professor Henry Marcus for his advice and comments.

Finally, I would like to express my sincerest thanks to Todd Taylor for the valuable time and experience he graciously donated whenever I sought advice.

TABLE OF CONTENTS

LIST OF FIGURES

LIST OF TABLES

Nomenclature

Mathematic Notation

d		fuel oil density
D		propeller diameter
DHP		delivered horsepower
EHP		effective horsepower
g		gravitational acceleration
G	$\frac{\Gamma}{2\pi \cdot R \cdot V_s}$	non-dimensional circulation
K_Q	$\frac{Q}{\rho \cdot \eta^2 \cdot D^5}$	torque coefficient based on rps
K_T	$\frac{T}{\rho \cdot \eta^2 \cdot D^4}$	thrust coefficient based on rps
M		number of vortex/source lattice nodes along the span
n		normal vector on a surface
η		propeller revolutions per second
n_H	$\frac{DHP}{SHP}$	hull efficiency
N		number of vortex/source lattice nodes along the chord
PC	$\frac{EHP}{SHP}$	propulsive coefficient
Q		propeller torque
QPC	$\frac{EHP}{DHP}$	quasi-propulsive coefficient
R		propeller radius
sfc		specific fuel consumption
SHP		shaft horsepower
T		propeller thrust
V		velocity
V_s		ship speed
Γ		dimensional circulation
ρ		density of fluid

Chapter 1

1 Introduction

The hydrodynamic design of marine propellers comprises two major tasks. First, a radial and chordwise distribution of circulation over the blades that will produce the desired thrust subject to appropriate constraints is established. Then, the shape of the blade that will produce this prescribed distribution is found.

Lifting-surface methods have become widely accepted as the most accurate way to determine the pitch and camber distribution required to generate a prescribed loading over the blades. Current trends in propeller design have led to complex blade shapes involving high skew and rake and extreme radial pitch distributions. The successful design of such propellers requires an extremely accurate lifting-surface computational procedure. Although techniques for direct blade shape determination using numerical lifting surface theory and assuming a hubless, ductless, single-stage propeller operating in potential flow have been widely used in the past, recent design concepts have rendered these assumptions invalid.

Historically, it is assumed that the propeller operates in potential flow. Potential flow theory provides a powerful basis for representing the propeller's own flow field but contains no mechanism to treat the so-called effective inflow problem which arises from the coupling of the propeller's induced velocity field to the vorticity in the incoming flow resulting from the highly rotational shear flows of the ship's boundary layer and wake in which propellers actually operate. Viscous flow methods capture the vortical phenomena of the inflow to the propeller but offer a poor framework for representing the propeller itself and manipulating its geometry. Modern propeller blade design methods couple viscous flow with potential flow, to rationally address the effective inflow problem.

The objective of this thesis is to develop a more efficient and robust algorithm for blade shape alignment as a part of a coupled lifting-surface combined design and analysis code for marine propulsors developed at Massachusetts Institute of Technology (MIT), known as *PBD-14*. Also, to investigate propeller fabrication and inspection methods, both traditional and modern, and examine the economic impact of propeller tolerances.

Chapter 2 provides the background of the propeller blade design process. In particular, it overviews the propeller blade design methodology and describes the blade shape manipulation procedure currently used in *PBD-14*, as well as the shortcomings of this scheme which lead to the need for a new blade shape alignment algorithm.

Chapter 3 describes the methodology behind the developed blade shape manipulation procedure. It presents the streamline tracing scheme and the method used for the evaluation of the geometry of the output blade, together with adjustments which are necessary for the new algorithm to be smoothly incorporated inside the existing design/analysis program.

Chapter 4 presents the blade design cases tested. For these design examples, the David Taylor Model Basin (DTNB) 4119 propeller [22,23] and the water jet 21 [6] were used as inputs. Both designs involved coupling of the design program with an Euler/IBLT flow solver, *MTFLOW*.

Chapters 5 and 6 address propeller inspection and manufacturing tolerances issues. In particular, Chapter 5 overviews the propeller manufacturing procedure, the existing tolerance systems and specifications, as well as several of the propeller inspection methods. Chapter 6 examines the economic impact of manufacturing an example propeller according to a certain tolerance system.

Finally, Chapter 7 includes the main conclusions drawn from this thesis for the new propeller blade alignment method and the propeller tolerances economics.

Chapter 2

2 Propeller Blade Design Overview

2.1 Introduction

PBD-14 is a potential flow, vortex-lattice combined design and analysis code that has evolved from many earlier generations of propeller design and propeller analysis programs developed at the Marine Hydrodynamics Laboratory (MHL) at MIT [1,2,3]. The *PBD-14* program is capable of the design and analysis of single and multi-stage open and ducted marine propulsors [4,5,6].

PBD-14 uses a vortex-lattice geometry, including blade thickness effects, to represent the propulsor blades [2,7]. The blade geometry is represented internal to *PBD-14* as a uniform cubic B-spline surface. The vortex-lattice mean camber surface and thickness of the blades is represented with piecewise constant vortex and source elements. Blade forces are computed using the Kutta-Joukowski's and Lagally's theorems [24]. The program can either function as a stand-alone code when provided

with an effective flow field or be coupled with a viscous flow solver for computing the effective wake problem [8,9].

The benefit of using a propeller code coupled with a flow solver can be summarized into the resulting ease with which the procedure supports multiple blade row cases. While in potential flow alone numerical difficulties occur as a result of the fact that wake sheet singularities from upstream blade-rows approach control points on the downstream blade-row, in the coupled viscid-inviscid procedure, all of the vorticity in the flow field is dealt with by the flow solver so that there are not singular structures, and the velocity field is smooth. Thus, *PBD-14* has to deal with only one blade row at a time.

2.2 Propeller Blade Design Background

The hydrodynamic design of marine propellers comprises two major tasks. First, a radial and chordwise distribution of circulation over the blades that will produce the desired thrust subject to appropriate constraints is established. Then, the shape of the blade that will produce this prescribed distribution is found. As a part of this second task, the process of designing a propeller blade basically consists in finding the shape of a surface, the mean camber surface, which carries a prescribed load distribution, such that the kinematic boundary condition $V \cdot n = 0$ is satisfied on that surface in the presence of a given flow.

Three different types of 'inflow' are identified in the context of *PBD-14* propeller design and analysis program:

1. The nominal inflow, which is defined as the velocity field in way of the propeller or blade-row of the propulsor when there is no propeller operating.
2. The total inflow, which is defined as the velocity field while the propeller is in operation, and
3. The effective inflow, which is defined as the total inflow less the propeller induced velocities.

The difference between the nominal and the effective inflows is due to vorticity being present in the nominal inflow. In the case of an irrotational nominal inflow field where there is no vorticity, there is no difference between the nominal and effective inflows.

The propeller blade design process currently integrated in *PBD-14* can be summarized into the following three steps:

1. Calculate the velocities induced at a set of control points on the blade by a prescribed spanwise and chordwise distribution of circulation and thickness using a vortex/source lattice method.
2. Adjust the blade shape until the normal component of the total fluid velocity (induced plus effective) at the set of those control points is minimized in a least-squares sense.
3. Compute the resultant distribution of force on the blade by using Kutta-Joukowski's and Lagally's theorems.

2.3 Blade Shape Representation Using B-spline Surfaces

The use of B-spline surfaces for blade shape representation is internal to *PBD-14* and offers a significant number of advantages versus other blade shape descriptions.

In order to find the shape of a surface that satisfies the kinematic boundary condition in a given flow, the designer first needs to manipulate the blade shape to be tangent to the local flow. Since the flow field changes as the blade shape is modified, the flow problem around the propeller/body combination given the new blade shape now needs to be solved. Thus, an iterative approach to the final shape is required and the process is continued until the blade shape converges. For this reason, the geometry of the blade needs to be described in a way that can be easily and robustly manipulated.

Although with the use of B-splines the description of the blade surface is done in a compact way, using a relatively small set of vertex points, this description is dense in the sense that the blade surface is known completely. This is not the case with other blade shape descriptions, such as parametric or tabular offset representations, which require interpolations to evaluate the surface at a general point. A set of vertex points describing a B-spline surface contains all of the information to uniquely define any point on that blade surface, together with its normal vector and curvature.

Another advantage that the representation of the blade using B-spline surfaces has is their suitability for transmission of the blade shape to other programs. The precise definition and format for transmission of B-spline surfaces to other programs are standardized [10]. B-spline surfaces can be interrogated at an arbitrarily fine mesh of points to define the blade. This way, the same B-spline can be used for both design and manufacture procedures to define geometry to the accuracy required in each case.

Finally, B-splines are convenient to use. The control polygon net that describes this family of surfaces can be quite small in the case of the camber surface of a propeller blade, with a 7 by 7 control polygon vertex grid being satisfactory in many applications. The B-spline surface is easy to manipulate during the design process because each B-spline vertex has a local effect. This way, the blade surface remains always well defined and effects of moving any vertex are localized, thus aiding convergence.

2.4 Current Blade Shape Manipulation Procedure in PBD-14

The blade shape manipulation process involves trying to find a blade shape that nulls $V \cdot n$, the normal component of the total flow velocity, on the blade. Since the blade shape is represented by a B-spline surface, the blade shape manipulation actually involves adjusting the location of the vertices of the B-spline's control polygon.

The current blade shape alignment scheme involves a set of iterations which are internal to *PBD-14*. At any of those iterations, each one of the vertices of the B-spline's control polygon is perturbed by a small known quantity. The algorithm then examines the quantity by which the normal component of the total flow velocity at each one of the prescribed control points changes as a result of this known perturbation. This way, the program solves for how much the B-spline's control polygon vertices need to move so that $V \cdot n$ will be zero at all the control points. Since this is an overdetermined system, the solution is obtained in a least-squares sense. As soon as an iteration of the design process is completed, the resulting B-spline net representing the blade can be used as input to the next iteration and so on. This process is repeated until the blade shape has finally converged.

Because of the localized effect that the displacement of a particular vertex of the control polygon of the B-spline surface has on the blade surface, the change in the normal velocity at a particular control point will be different than the change caused by the same vertex displacement at any other control point. This way, an overdetermined set of linear equations for the required displacement of each control polygon vertex can be defined. The coefficient matrix elements of this set of equations therefore are the changes in $V \cdot n$ at each control point, because of the small prescribed change in the position of each one of the B-spline control polygon vertices. The right hand side of the set of equations contains the normal velocities at each control point. As previously mentioned, this system can be solved in a least-squares sense to obtain the necessary vertex displacements so that $V \cdot n$ is minimized at each control point. This resulting surface however is not necessarily the desired one, as the elements of the coefficient matrix depend on the shape of the initial surface in a non-linear way. Therefore, the process is repeated until the blade shape has converged.

Another issue that is of particular importance is the way that the control polygon vertices of the B-spline net are allowed to move. During any blade shape manipulation procedure, the gross properties of the blade shape (such as chord lengths, for example) have to be maintained, and any changes in those characteristics have to be kept at a

minimum. To achieve this, the control polygon vertices are only allowed to move on cylindrical surfaces parallel to those defining the axisymmetric flow grid and in a direction normal to the inflow direction as defined by the propeller advance coefficient. This way, control polygon vertices for stators will be perturbed in a mostly circumferential direction, whereas vertices for lower pitch blades will be moved closer to an axial direction.

The blade surface that satisfies the condition of zero normal velocity is not unique, as a surface which is required to pass through an arbitrarily chosen curve in space can always be found. Traditional methods require that the midpoints of the section nose-tail lines at each radius lie on a particular space curve defined by the rake and skew, something that would be difficult to implement with a B-spline representation of the blade surface.

The current blade shape manipulation procedure requires that a particular spanwise row of control points remain invariant. This can in many cases be the first row, so that the blade leading edge curve remains fixed. However, as the blade shape is manipulated, the rake, skew, and chord length can also be changed as a result. Although these changes can be small, a designer may need to extract the rake, skew, and chord length values for the current blade, adjust as required, and create a new B-spline surface to repeat the process.

Since the inner and outer extremities of the B-spline surface do not pass through the vertices, except those at the leading and trailing edges, keeping the vertices on the centerbody and tip streamtubes does not ensure that the blade surface will lie along these surfaces. For this reason, during each blade shape iteration, a radial adjustment is made to the inner and outer row of vertices in order to place the inner and outer edges of the blade surface as close to the centerbody and tip streamtubes as possible. This refinement not only prevents any geometrical mismatches from occurring, but also stabilizes the blade shape iteration process.

2.5 *The Need for a New Blade Shape Manipulation Algorithm*

The algorithm for adjusting blade shape in the current version of *PBD-14*, described in the previous paragraph, works well in most of the cases. However, in the cases which involve more complex schemes such as highly tapered afterbodies, ducted propulsors and/or higher load distributions, the process has to be carefully monitored by the user. The design procedure is controlled by several "design parameters" which have to be input by the user. Therefore, some manual intervention and user expertise is required.

As previously mentioned, in the current blade shape adjustment scheme in *PBD-14*, each one of the vertices of the B-spline's control polygon is perturbed by a small known quantity at each iteration. This quantity is set by the user. However, the overall displacement that a particular control polygon vertex is allowed to move in a single blade iteration is restricted for stability reasons and cannot exceed a certain quantity, which is also a user's input. This way, the blade cannot achieve its final shape so as to satisfy the kinematic boundary condition in one run and usually several iterations are needed. This slows down the design process considerably.

Another problem that was identified earlier in the development of *PBD-14* is that, during the blade shape manipulation procedure, the blade surface can develop corrugations in the spanwise direction. Figure 2-1 demonstrates the case. DTMB Propeller 4119 is used as an example. An 11 by 11 B-spline net is used to describe the propeller blade surface. Figure 2-1 shows the input B-spline net for the 4119 propeller, as well as the output B-spline net produced by the design procedure in *PBD-14*, using a notional but smooth circulation distribution. As can be seen from the output case plot, the blade surface develops intense spanwise corrugations which result in a distorted final blade shape.

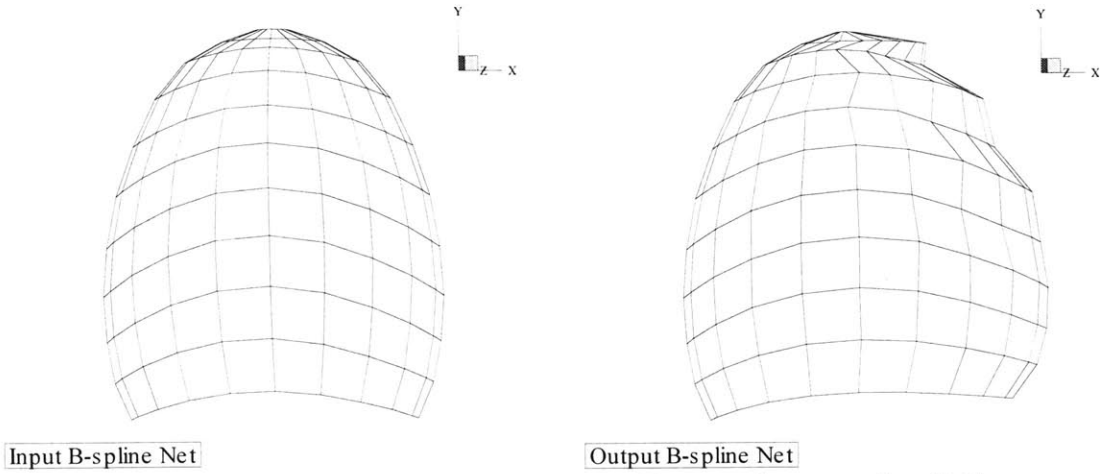

Figure 2-1. Design input and output B-spline nets for propeller 4119.

This problem was partially overcome by adding a penalty function to the least-squares solution for the position of the B-spline vertices related to the spanwise rate of change of curvature. This penalty function is imposed on the blade design procedure by means of a weighting given to the blade smoothing equations in the alignment matrix. The blade shape algorithm minimizes $V \cdot n$ at the control points. In addition, the current blade shape algorithm minimizes the spanwise components of the normal at the control points. By penalizing spanwise components of the normal, the blade shape is "ironed flat" in the spanwise direction. This results in a fair output B-spline net, as shown in Figure 2-2, and consequently a smoother blade shape.

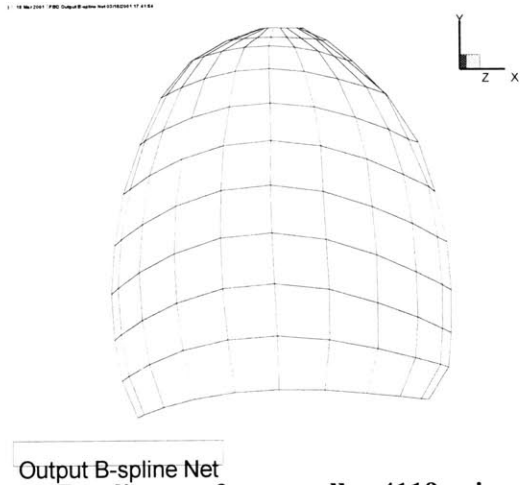

Figure 2-2. Output B-spline net for propeller 4119 using penalty function.

Penalizing the least-squares solution results in a fairer output blade shape, which deviates though from the actual solution needed to satisfy the kinematic boundary condition constraint imposed on the design. Thus, more iterations are needed to obtain a blade shape that is smooth and close to the functional performance required, even though less correct in a hydrodynamic sense, and the whole design procedure becomes slower. In addition, the weight that penalty function carries differs from one case to another and cannot be preset. Thus, it depends on the user to monitor the process and decide on the right weight to use for the penalty function.

For all the reasons discussed in this chapter, the need for the development of a more efficient and robust algorithm for adjusting blade shape in *PBD-14* design mode becomes apparent. This new algorithm is envisioned to overcome the amount of manual intervention the current blade shape manipulation method needs, as well as its known shortcomings, and result in a highly efficient propeller blade design adjustment scheme.

Chapter 3

3 A New Blade Shape Manipulation Procedure

3.1 Overview

As discussed previously, the process of designing a propeller blade involves the manipulation of the blade shape so that it would be tangent to the local flow. One way to approach this is to require the blade mean camber surface to exactly match the streamlines of the local flow field in which the blade operates. This can be accomplished through a process that consists of the following three steps:

1. Calculate the velocities induced at a set of control points on the blade by a prescribed spanwise and chordwise distribution of circulation and thickness using a vortex/source lattice method.
2. At a set of vortex/source lattice grid points lying on a "generator line", trace the streamlines of the local flow field in which the blade operates by calculating the total velocity at these points.
3. Fit the blade mean camber surface so that it matches those streamlines.

The procedure used in the first step is an extension of the vortex lattice method presented in [3]. The given continuous vortex and source sheet strengths are first discretized into a lattice of spanwise and chordwise elements. The elements are of constant strength and the endpoints of each element are located on the blade mean surface. The spacing of the discrete elements and the relative location of the control points are critical to the accuracy of the method. One first finds M points along the leading-edge curve with 'cosine spacing' in arc length. Each of these points serves as the origin for a streamline which lies on the blade surface and is parallel to the streamtubes used in the axisymmetric flow solver. Note that these streamlines do not in general coincide with the streamlines referred to in this study and which are the streamlines of the local flow field in which the blade operates and are used in this method for the blade shape manipulation process. Next, one obtains N points along each streamline, again with cosine spacing in arc length. The resulting set of M by N points serves as the nodes for the vortex/source lattice.

3.2 Total Velocity Calculation

To trace the streamline that passes from a certain vortex/source lattice grid point requires that the total velocity at this point is known. As discussed in the previous chapter, the total inflow is defined as the velocity field while the propeller is in operation. This contains the inflow velocities from the axisymmetric flow solver, velocities due to the propeller blade rotation as well as the propeller induced velocities. The axial, radial, and tangential components of the inflow velocities are evaluated at the vortex/source lattice nodes by linear interpolation from an axisymmetric grid of RANS points at which the respective components of the inflow velocities are known. Then, these velocities are converted into velocity components in Cartesian coordinates where the components resulting from the propeller rotation are added.

To complete the total velocity calculation, the blade-induced velocities are also needed. The induced velocity at each control point on the blade can be computed once the

positions and strengths of all the discrete vortex/source elements comprising the initial vortex/source lattice grid are determined [3]. However, the actual induced velocity at each node used for the streamline tracing procedure is not known. To deal with this problem, the algorithm takes advantage of the fact that the number of spanwise vortex elements and the number of the control points over the chord of the blade are equal. This way, it is assumed that the average of the induced velocities at two consecutive control points in the spanwise direction can be used without significant error to represent the induced velocity at the vortex/source lattice node that lies between those control points and is characterized by the same chordwise number N. In the spanwise direction however, the number of control points is always less than the number of nodes by one. Therefore, to calculate the induced velocities at the tip most nodes of the vortex-source lattice grid, only the induced velocities at the tip most set of control points are used. The same approximation also holds for the grid points lying at the root of the blade, where the load induced velocities calculated at the root most set of control points are used. It is obvious that the error introduced into the total velocity calculation at the vortex/source lattice grid points because of the previous assumption is reduced as the grid becomes finer and more control points are used.

The design technique described here was improved by incorporating a more accurate total velocity calculation scheme. Since load induced velocities are only known at a set of control points, the algorithm was restricted by the discretization available for the control point or the vortex-source lattice grid. This was soon proved to be insufficient for the accuracies required by the streamline tracing design method. Figures 3-1 and 3-2 demonstrate the case. Figure 3-1 shows the solved versus the design spanwise circulation distribution for a DTMB 4119 single open propeller in uniform flow for a very coarse vortex-source lattice grid of 11 by 15 nodes whereas Figure 3-2 shows the same results for the finest grid available, using 41 by 41 vortex-source lattice nodes. Although the output blade shape in both cases was smooth, with no presence of spanwise corrugations, the resulting solved circulation distribution deviates significantly from the design load, in particular throughout the smaller radii and especially in the case where a coarse grid was used. Results are significantly improved with the finer grid, as shown in Figure 3-2.

However, given that the finest discretization available was used for the later case without producing highly accurate results, the need for a more accurate scheme becomes apparent.

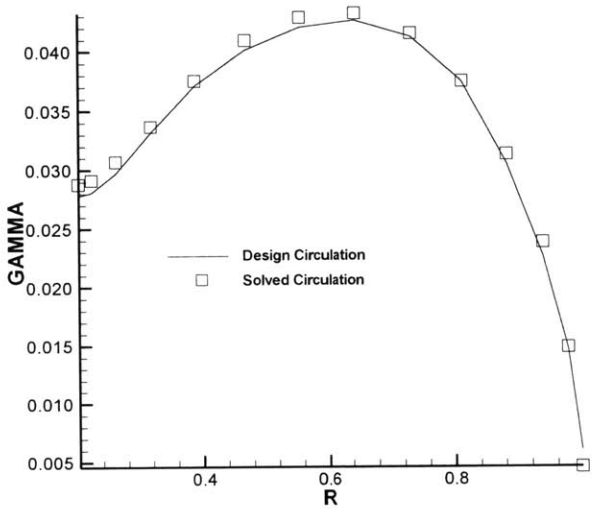

Figure 3-1. Comparison of design and solved spanwise circulation distribution for single open propeller (coarse grid).

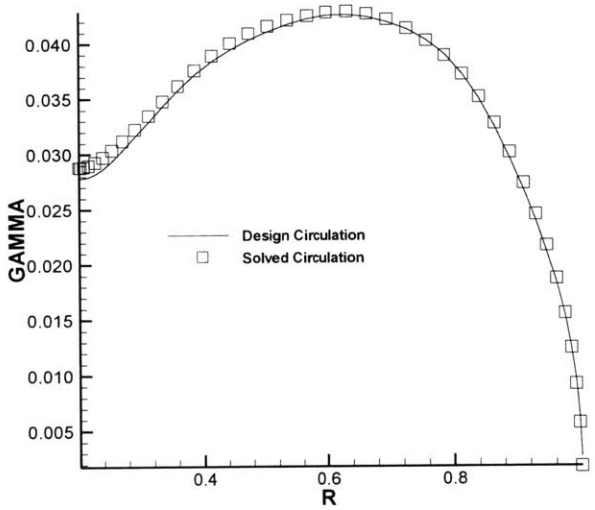

Figure 3-2. Comparison of design and solved spanwise circulation distribution for single open propeller (fine grid).

The improved total velocity calculation scheme consists in fitting the load induced velocities interpolated at a particular chordwise strip of grid points with a spline

and then, evaluating this spline at multiple points over the chord, to find load induced velocities at the new points. These new points can be seen as internal steps between adjacent vortex/source lattice nodes. As inflow and rotational velocities can also be evaluated at these internal points or steps the same way it was previously discussed, the technique results in a very fine discretization capability in the chordwise direction. Thus, total velocity can now be calculated at a significantly increased number of points at a particular chordwise strip on the blade. This is proved to significantly improve the accuracy of the design method, as shown in Figure 4-4 in the following chapter.

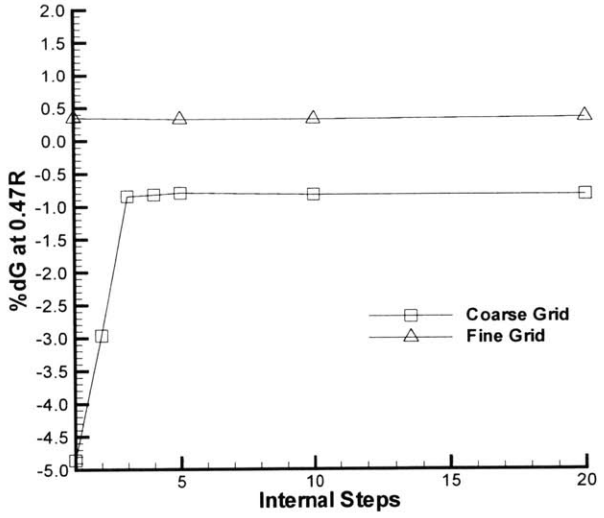

Figure 3-3. Percent error in solved circulation at .47R versus number of internal steps.

The effect of this internal discretization is shown in Figure 3-3. This figure shows the percent difference between the solved and the design circulation at a particular radius of the blade of a DTMB 4119 single open propeller in uniform flow versus the internal number of points or steps used for the disrcetization, for two different initial vortex/source lattice grids: a coarse one, with 15 by 15 nodes, and a fine one, with 35 by 35 nodes. As can be seen in Figure 3-3, the error in the prediction of the solved circulation when a very fine vortex/source lattice is used is almost independent of the number of the internal steps from node to node, as the initial fine blade discretization already provides for increased accuracy. In the case of the coarse vortex/source lattice grid, as expected, the error is reduced to a minimum value, as the number of internal

steps increases. This minimum is, in absolute values, larger than the respective minimum prediction error in the case of the fine grid because of the inaccuracies introduced by the use of a coarse vortex/source lattice grid. However, it is shown that, in general, a small number of internal steps is sufficient for a satisfactory blade design. Finally, since only directional information rather than actual total velocities is needed for the streamline tracing to be accomplished, the three dimensional total velocity calculated at each internal point/node is subsequently normalized. This is because the step used in the growth process takes care of the necessary distance to grow based on required chord lengths. Thus, multiplying the step by the normalized velocity components and adding to the starting point, the end point Cartesian coordinates can be found.

3.3 Tracing Streamlines

As is the case with the existing blade design algorithm used in *PBD-14*, the geometry of the blade surface is described by a B-spline surface, for the benefits that a B-spline surface representation has, as discussed in the previous chapter. However, finding a blade surface such as it matches the streamlines of the local flow field in which the blade operates would be difficult to achieve by manipulating the B-spline surface net which is used for the blade description. Instead, the direct way to accomplish this task is to directly manipulate the geometry of the mean camber surface which describes the blade.

In order to initiate the streamline growing procedure, a generator "line" from which to grow upstream and downstream on the blade surface is needed. This "line" is a polygon line formed by the set of the endpoints of the discrete spanwise vortex/source elements which are defined by the same N number along the streamlines that are parallel to the streamtubes in the axisymmetric flow solver. As a result, this generator line can lie anywhere along the chord of the blade where the N spanwise vortex/source elements lie. In the blade design method discussed in this chapter, the user can select the generator line from where the streamline tracing procedure starts and eventually the output blade is

formed. Because of the fact that this is a "one step" method, in the sense that there are no internal blade shape iterations as was the case with the previous blade design scheme in *PBD-14*, and the generator line is a "curve" in space, it might be desirable to select the generator line to be somewhere close to the blade midchord line. This way, blade shape fluctuations that result from abrupt movement of the blade can be reduced.

An important issue, which characterizes the blade shape adjustment by means of the streamline tracing method, is the right interval or step to be used in the blade growth process. As is also the case with the current blade shape adjustment scheme in *PBD-14*, it is necessary for the designer to maintain the gross properties of the blade shape. During any blade shape manipulation, potential changes in blade shape characteristics must be kept to a minimum. In the blade design algorithm currently used in *PBD-14*, the blade surface is described by a B-spine net. Therefore, preserving the gross properties of the blade is achieved by allowing the control polygon vertices of the B-spine net to move in a certain direction only.

In order to maintain the gross geometric properties of the blade shape with the developed blade shape adjustment scheme, the manner in which the size of the interval or step that is used in the streamline growing process is calculated had to be carefully considered. This step is calculated by computing the distance between two adjacent vortex/source lattice nodes in three dimensions, using the Cartesian coordinates of the nodes. This distance is in general different from one set of two grid points lying along the same streamline to the next set of two grid points on that same streamline, but is exactly identical for each corresponding set of two adjacent grid points between the input and the output blade. This way, the streamline growing process leads to an output surface, which has exactly the same number of nodes defining the vortex/source lattice, spaced at the same intervals as the input blade.

The use of the endpoints of the discrete vortex/source elements that represent the input blade surface in the definition of the streamline growing step involves one discrepancy. As described earlier, each one of the M points along the leading edge of the

input blade serves as the origin for a streamline which lies on the blade surface and is parallel to the streamtubes used in the axisymmetric flow solver. In other words, the N points obtained along each one of those streamlines in the chordwise direction lie on streamlines which are generated by only taking the axisymmetric inflow into account. These differ from the real streamlines which result from the total flow field in which the blade operates, which also consider blade rotation and load. As a result, the gross blade characteristics are only maintained in a "streamline" sense. Because of the difference between the streamlines which are parallel to streamtubes and the real streamlines that result from the local flow field in which the blade operates, there are also minor differences in the blade shape characteristics between the input and the output blade.

This problem is overcome by using the output blade grid point coordinates as a reference for the growth step computation. As described in the previous chapter, the process of designing a propeller blade is iterative. Since the blade surface does not sit passively in the flow field but changes it as its shape is modified, the flow problem around the propeller/body combination has to be solved again, as soon as the blade shape is manipulated and so on. During each iteration, the algorithm uses information for the location of the vortex/lattice grid points created during the previous iteration, when the nodes were placed on actual streamlines. In particular, for the first run of the code in design mode, such information does not exist yet but can be created by going through an analysis run before the actual design runs start. A run of the code in analysis mode before the actual design starts will create the information needed, without altering the blade shape. This way, it is ensured that the blade shape characteristics are maintained throughout the whole design process.

3.4 Treatment of the Viscous Sub-layer

To aid generation of the streamlines to which the blade surface will subsequently be fit, the algorithm allows for velocity gradients that are typical of a viscous sub-layer along the hub or duct, if they are present. Thus, the user can specify the number of cells

close to the hub or duct in which the velocities in the input velocity file which typically comes from a RANS solution are substituted with values that represent velocity out of the viscous sub-layer. Naturally, this is not a realistic representation of the RANS flow field for the rest of the blade-row problem, but is necessary for a discretized representation of what in reality the streamlines of the local flow field in which the blade operates would look like.

As a result of this capability however, the streamline growing process has to be treated separately for a predefined "upper" and "lower" part of the blade. If the process was to be developed in a monotonic manner, from the blade root to the blade tip or vice versa, the vortex/source lattice grid points in and on the verge of the viscous sub-layer at which to interpolate the inflow velocities would not be known yet, as they would not have been traced up to this point. This has to do in particular with the nodes contained in the hub sub-layer, in the case of a process from the root to the tip of the blade, and the nodes in the duct sub-layer, for a growing process from the tip to the root of the blade. For this reason, and depending on the number of hub and/or duct cells that the user specifies to be treated as a viscous sub-layer, the algorithm automatically selects a node in the spanwise direction to start the streamline growing process. This first node lies naturally on the generator line in a chordwise sense, as described further on, but also in a region along the span of the blade which is free of any viscous sub-layer type velocity gradients. The process is then repeated in an identical manner for the two "halves" of the blade along the span.

3.5 The Use of Euler's Method

The blade shape design method introduced here implements the modified Euler's method for numerical integration of differential equations (average slope) to find the vortex/source lattice nodes locations in Cartesian coordinates [11]. This method gives a numerical solution of improved accuracy compared to the forward or the backward

Euler's methods by using the average of the derivative at the initially computed end points of the interval or step.

Consider a first-order ordinary differential equation of the form

$$\frac{dy}{dx} = f(x,y) \text{ subject to } y = y_0 \text{ at } x = x_0 \tag{3-1}$$

For this case, a Taylor series expansion has the form

$$g(x) = g(x_0, y_0) + (x - x_0) \cdot g'(x_0, y_0) + \frac{(x - x_0)^2}{2!} \cdot g''(x_0, y_0) + \ldots \tag{3-2}$$

The Taylor series of (3-2) can be truncated so that only the term with the first derivative is used. Thus, Euler's method suggests that the value of the dependent variable can be computed using

$$g(x) = g(x_0) + (x - x_0) \cdot \frac{dy}{dx} + e \tag{3-3}$$

The derivative $\frac{dy}{dx}$ in (3-3) is evaluated at the beginning of the interval. It is evident that as the distance or interval $(x - x_0)$ increases, the error e increases because the nonlinear terms of the Taylor series expansion in (3-2) become more important. Thus, it is important to keep the distance $(x - x_0)$ small.

Using the Euler's method for the streamline tracing method of blade shape adjustment, and for a growing process in the x-direction, $g(x)$ and $g(x_0)$ in (3-3) can be thought of as the end and the start point x-direction coordinates respectively; $(x - x_0)$ represents the interval or step used in the growing process and the derivative $\frac{dy}{dx}$ the x-component of the total velocity at the start point. The process is then repeated in a similar manner for the y and z directions.

The modified Euler's method instead uses the average of the total velocity at the initially computed end points of the interval or step. For each successive interval, the procedure with the modified Euler's method that the algorithm described here uses is as follows:

1. Evaluate the total velocity at the start of the interval.
2. Estimate the value of the location of the node (dependent variable) at the end of the interval using the Euler's method.
3. Evaluate the total velocity at the end of the interval.
4. Find the average total velocity using the total velocity values of steps 1 and 3.
5. Compute a revised value of the location of the node at the end of the interval using the average total velocity of step 4 with Euler's method.

As highlighted before, it is important to keep the step in the growing process small, as this way the error in the grid points location estimation will be smaller. Therefore, the finer the vortex/source lattice grid used, the smaller the error in the final output. The obvious drawback though of having to use a very fine vortex/source lattice grid is that the whole design process is slowed down significantly as it becomes computationally intensive.

The modified Euler's method is used in this algorithm for all the vortex/source lattice grid points over the chord of the blade, except those lying exactly on the leading and trailing edge. This is because load induced velocity information is not available for these end points and thus, the aforementioned scheme cannot be applied. Instead, the backward and forward Euler's methods that are used for the leading edge and the trailing edge points respectively are assumed to provide the end points coordinates in three dimensions with sufficient accuracy.

3.6 *Blade Fitting and Fitting Error*

As soon as the streamlines of the local flow field in which the blade operates are traced, the new vortex/source lattice grid points are placed on those streamlines in the same fashion as was previously described. Hence, a new blade surface that matches the streamlines of this flow field is generated. The whole blade shape manipulation therefore takes place by directly adjusting the actual mean camber surface of the blade, represented by the vortex/source lattice. No modification to the B-spline surface representing the blade shape has been made yet. Therefore, it is necessary to create a perturbed B-spline net which will sufficiently represent the new "streamlined" blade surface.

Fitting a B-spline surface to the set of (x,y,z) points is accomplished through an automated scheme previously developed by MIT MHL for this purpose. This algorithm was developed to fit propeller blades with B-spline surfaces in a consistent manner [25]. Although there is no guarantee that this system is robust, experience with a number of varied blade geometries is encouraging. The accuracy of the fit can be judged in part by viewing a contour map of the approximate deviations of the input and fitted surfaces for a typical propeller. Figure 3-4 shows the deviation between the input and the B-spline fit for a variant of the DTMB 4119 propeller with an 11 by 11 B-spline net.

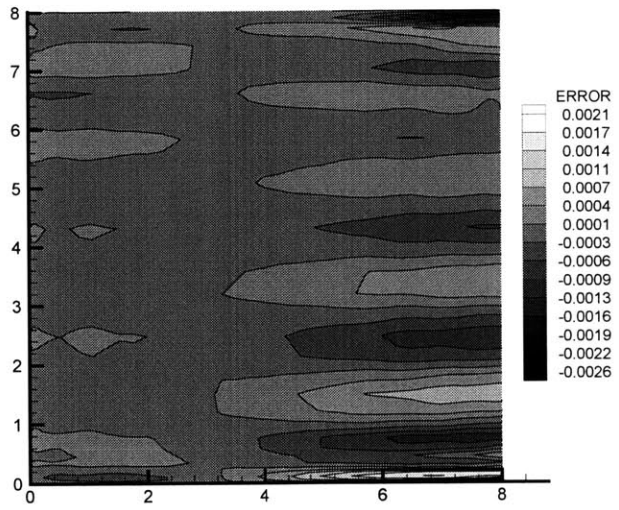

Figure 3-4. Contours of blade shape fitting error.

As far as accuracy in fitting existing data with a B-spline is concerned, one can potentially achieve any degree of accuracy in representing the blade surface with a sufficiently large number of vertices. Even though chord and skew distributions can be sufficiently represented by a very small number of vertices, this is not the case with pitch, camber and thickness, which govern the blade sections. As shown in [8], seven to nine vertices are needed to match the desired load distribution to a sufficient extent. In general, a small number of vertices generate a smoother surface, whereas a larger number is unnecessary and introduces the possibility of unwanted inflections in the blade surface.

As discussed in the previous chapter, the surface which satisfies the condition of zero normal velocity is not unique. In the existing shaping algorithm in which the blade surface is represented using a B-spline surface, this is accomplished by requiring that a selected spanwise row of control polygon vertices, usually those describing the blade leading edge, remain invariant. In the new blade shape manipulation method described here, the vortex/source lattice grid points which lie on the generator line remain invariant. This is consistent with traditional methods which require that the midpoints of the section nose-tail lines at each radius lie on a particular space curve defined by the rake and the skew, especially in the case where the generator line is selected to be close to the midchord line of the particular blade. However, with the design scheme discussed here, there is little likelihood that the output blade B-spline net resulting from the fitting process will end up having the tip most vertex of the leading edge exactly at $(x,r) = (0,1)$ in the axisymmetric solver's grid. Therefore, the output B-spline net of the perturbed blade surface is scaled so that the leading edge vertex of the tip lies exactly at $(x,r) = (0,1)$. This scaling of the B-spline net and, in consequence, of the blade surface itself is done in a three-dimensional sense and does not alter the principal geometric characteristics of the blade.

Finally, as is the case with the design algorithm currently incorporated in *PBD-14*, a radial adjustment is made to the inner and outer row of vertices of the output blade surface after it has been fitted with a B-spline net and scaled, in order to place the inner and outer edges of the blade surface as close to the centerbody and tip streamtubes as

possible. The scope here is twofold. First, as has already been discussed, simply keeping the B-spline net vertices on the centerbody and tip streamtubes does not ensure that the blade surface will lie along these surfaces. Second, in the new blade design algorithm presented here, the streamline growing process uses the vortex/source lattice grid points. In the spanwise direction of the blade though, the extremities of the lattice are inset one quarter interval from the ends of the blade, with this interval being equal to the radial interval from the hub to the tip of the blade, divided by the M trailing vortices across the span [3]. Thus, after each blade shape manipulation, the new B-spline net is fitted on an output blade surface which is shorter in the spanwise direction than the input blade surface by one half interval. Hence, after consecutive blade shape iterations with no radial adjustments, the change in gross dimensional characteristics of the blade would be significant. However, by making this radial adjustment, the extremes of the output blade surface are placed as close to the centerbody and tip streamtubes as possible within the same run, thus preventing any potential radial "shrinkage" of the blade from occurring.

Chapter 4

4 Validation

4.1 Design Examples

To demonstrate the capability of the new design approach introduced in this thesis, three design examples are presented. The first one involves designing a single open propeller stand-alone, i.e., no coupling with a flow solver is considered. The other two design examples involve the design of the same single open propeller and that of a water jet, both coupled with a flow solver. In these last two examples, the flow solver used is *MTFLOW*. *MTFLOW* is a system of programs for the viscous/inviscid design and analysis of axisymmetric bodies. Coupling *PBD* with *MTFLOW* implies that information created by one code is passed to the other code in an iterative process, thus allowing the user to solve for the flow characteristics created by a specified propulsor.

4.1.1 Single Open Propeller Stand-alone Design

This design example includes the stand-alone design of a single open propeller. Since the blade shape manipulation method introduced in this thesis is based on a fundamentally different principle than the method previously used in *PBD*, a relatively simple design case such as the stand-alone design of a single open propeller was considered important to be examined first, before coupling with a flow solver was introduced. A picture of the resulting geometry is shown in Figure 4-1. The starting geometry that is used for this case is DTMB 4119 propeller, which is given a smooth spanwise circulation distribution.

As was discussed in the previous chapter, the blade shape alignment method introduced here is a "one-step" method: no internal blade shape iterations occur while the design code runs. The design code was itself iterated several times before a final converged design was reached. The propeller characteristics at the end of each pass through the blade design procedure are shown in Figure 4-2. It has to be noted that blade shape convergence was achieved significantly faster with the new design scheme, compared to the existing technique used in *PBD-14*.

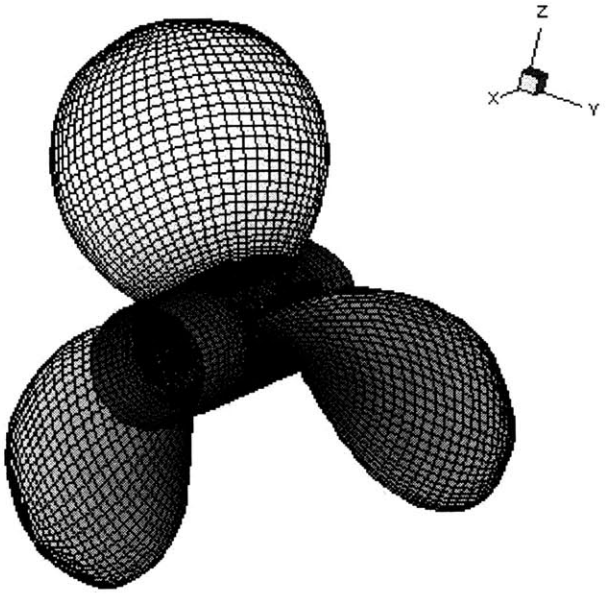

Figure 4-1. Notional single open propeller (stand-alone design).

Figure 4-3 shows that the normal component of the total velocity on the control points is minimized to a very good extent, except probably at the region close to the tip of the blade. This is because of the way the total velocities are considered at the tip-most region of the blade, in order to assist creation of a smooth final blade design.

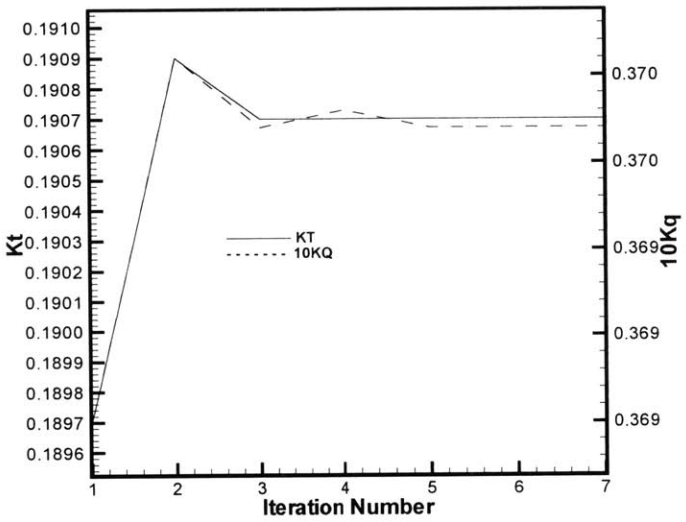

Figure 4-2. Convergence of K_T and K_Q for single open propeller (stand-alone design).

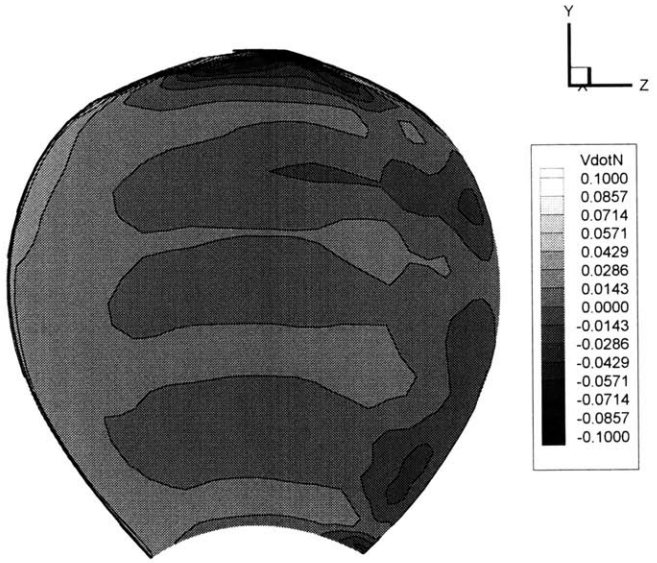

Figure 4-3. Contours of the normal component of the total velocity at the control points.

The final blade geometry that came out of the design process was consequently analyzed in *PBD-14*, to demonstrate the accuracy of the design method. The solved circulation distribution over the radius of the blade is compared to the design circulation distribution.

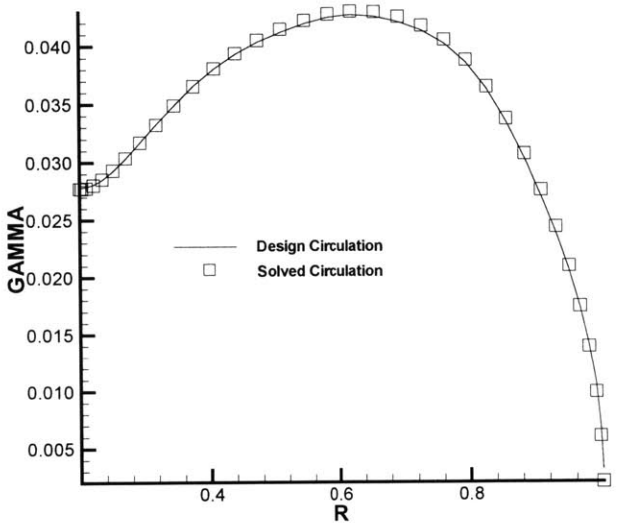

Figure 4-4. Comparison of design and solved spanwise circulation distribution for single open propeller (stand-alone analysis).

As shown in Figure 4-4, there is a considerably good agreement between the design and the solved radial circulation distribution on the blade.

4.1.2 Single Open Propeller Coupled Design

In this design example, the same single open propeller as in the previous example was used, except in this case coupled with a flow solver, *MTFLOW*, as discussed previously. Iteration between the axisymmetric flow solver and the propeller design code was performed 10 times. However, as can be seen in Figure 4-5, no modifications in the blade alignment occur after practically the 5^{th} iteration, where the designed blade can be considered converged. Figure 4-6 shows the resulting blade geometry. As can be seen, the new blade shape manipulation scheme results in a very smooth blade shape, without

any sign of shape corrugations in the spanwise direction, as was the case with the existing design algorithm in *PBD-14*.

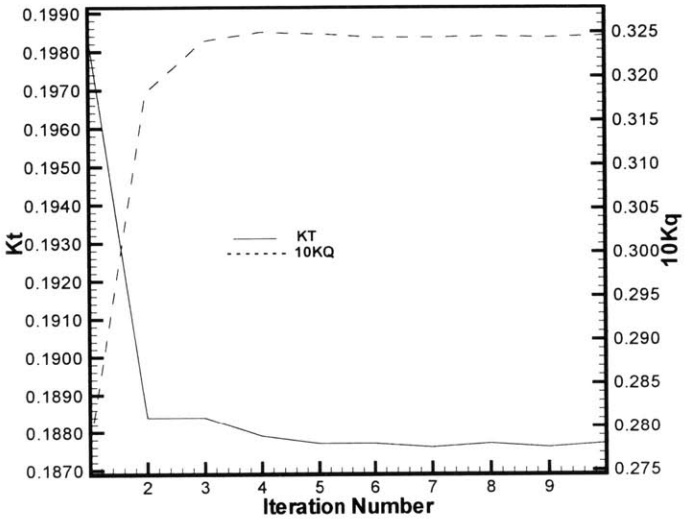

Figure 4-5. Convergence of K_T and K_Q for single open propeller (coupled design).

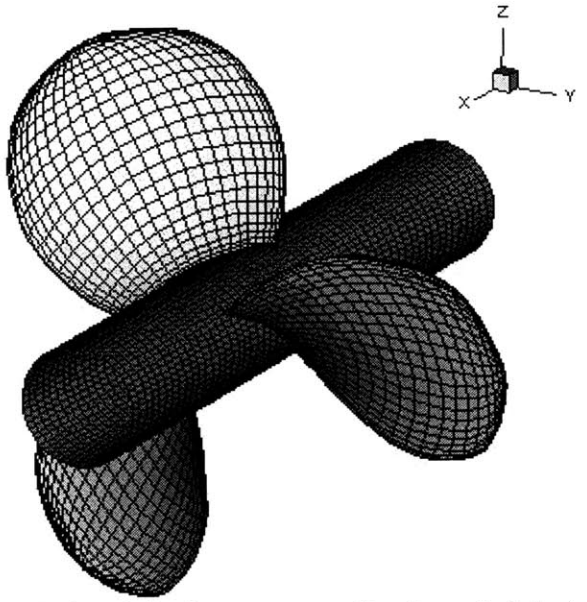

Figure 4-6. Notional single open propeller (coupled design).

As in the previous example, the final blade shape resulting of the design procedure was consequently analyzed. Coupled analysis runs were performed 10 times. Convergence was achieved after 7 runs, as shown in Figure 4-7. The radial distribution of

the solved circulation versus the design circulation is shown in Figure 4-8. In this case, the solved radial circulation distribution is slightly underpredicted versus the design case.

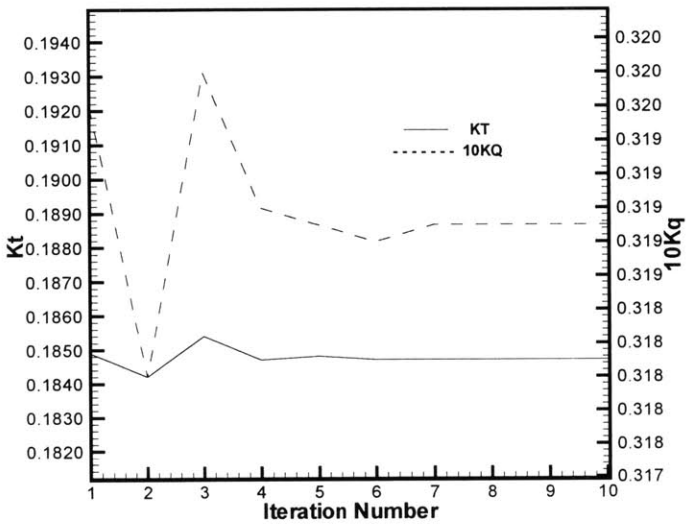

Figure 4-7. Convergence of K_T and K_Q for single open propeller (coupled analysis).

Some discrepancy is to be expected because of the additional complication in the design/analysis scheme that is introduced because of the coupling of both procedures with the axisymmetric flow solver. However, the reason of the discrepancy in this case might need to be further investigated.

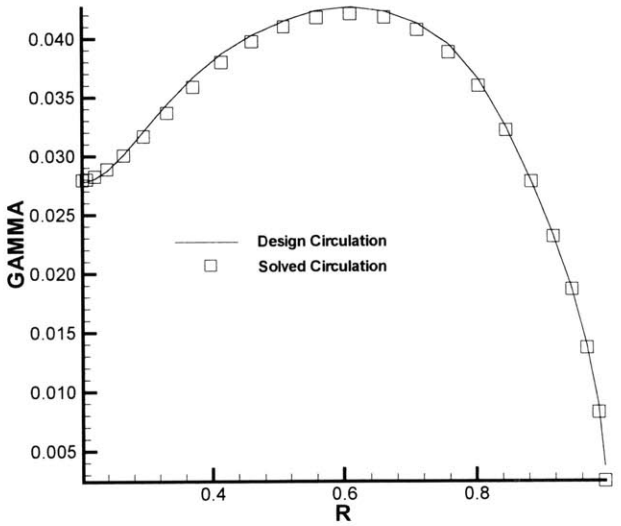

Figure 4-8. Comparison of design and solved spanwise circulation distribution for single open propeller (coupled analysis).

4.1.3 Water Jet Coupled Design

The final design example demonstrates the coupled design of a water jet. This comes as the next step after the single blade row propeller of the previous examples, as it involves a more complicated propulsor scheme with two blade rows, a rotor and a stator. Water jet 21 is the starting geometry that is used for this design example case.

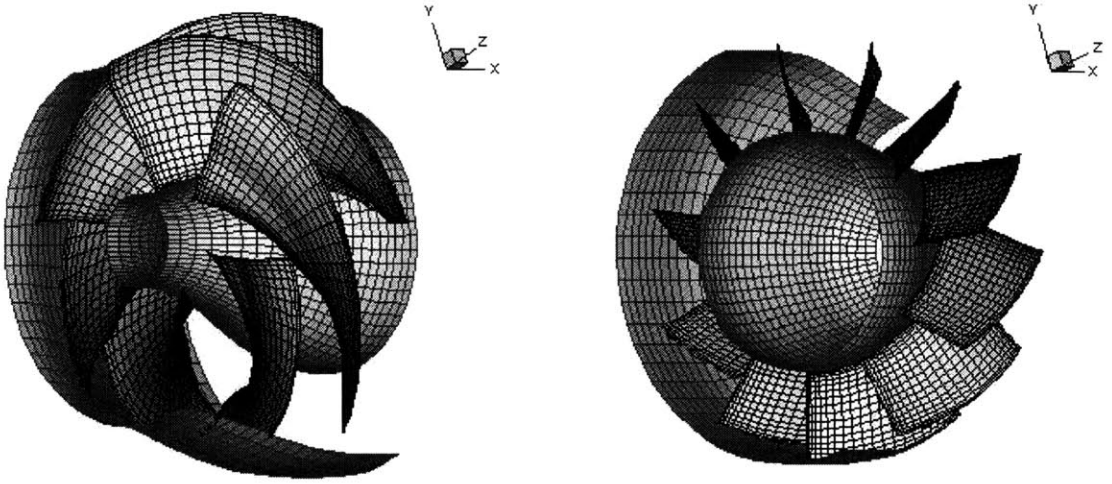

Figure 4-9. Notional water jet rotor (left) and stator (right) (coupled design).

Figure 4-9 shows the resulting geometry for the water jet rotor and stator. Similarly to the previous examples, the final design blades are fair, with no spanwise corrugations present.

Figure 4-10 shows the convergence of K_T and K_Q for the water jet rotor, during coupled analysis runs. Convergence was achieved after 10 *PBD-MTFLOW* iterations. The solved spanwise circulation distribution is then compared to the design circulation distribution. As shown in Figure 4-11, the design and the solved radial circulation distribution on the water jet rotor blade are in good agreement.

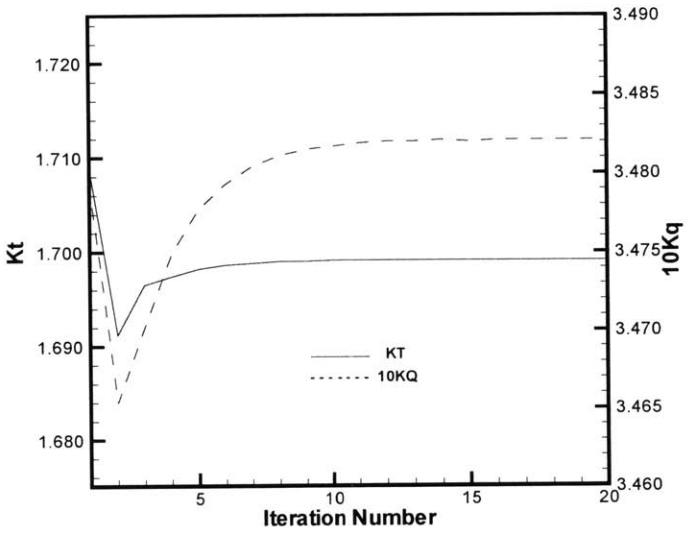

Figure 4-10. Convergence of K_T and K_Q for water jet rotor (coupled analysis).

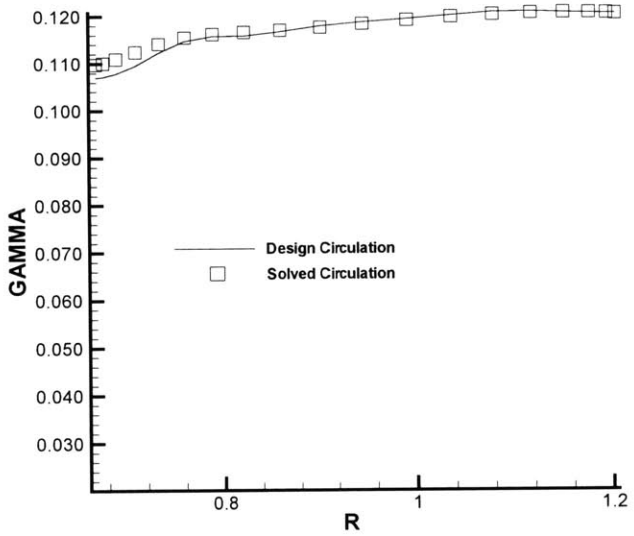

Figure 4-11. Comparison of design and solved spanwise circulation distribution for water jet rotor (coupled analysis).

Chapter 5

5 Propeller Inspection and Manufacturing Tolerances

5.1 Overview of the Propeller Manufacturing Procedure

In the last decades, significant progress has been made in the field of propeller design. Lifting surface methods have been widely accepted as the most accurate propeller design tool and are being applied to the unsteady cavitating flow problem [12]. This has led to the current trend in propeller design towards more complex blade shapes. This trend can be attributed to current trends in ship design towards higher shaft horsepower and propeller loading, use of nozzles and wake changing devices, as well as an increased demand for better efficiencies and reduced vibration and inboard noise level. However, propulsion problems can occur, mostly because of the traditional ship design procedure which relegates the detailed propeller design to the final ship design phase.

Another issue that constraints the propeller design is the manufacturer's capabilities. Ideally, advancements in design are accompanied by improvements in manufacturing. Nowadays, more powerful production tools are available, especially in

the fields of mechanization, computerized information and quality control. Numerically controlled (NC) machining and robotics represent a considerable improvement in manufacturing capability, from a technical point of view.

Figure 5-1 illustrates the basic sequence of propeller manufacturing events.

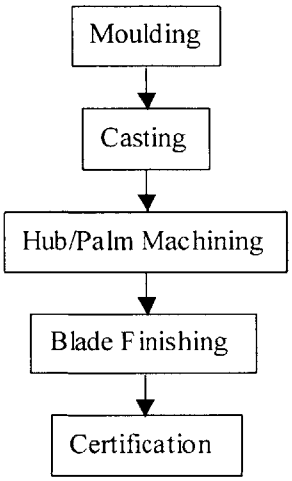

Figure 5-1. The sequence of propeller manufacturing events.

Propellers can be manufactured in a variety of materials to meet diverse customer needs. Standard alloys include:

1. Manganese Bronze
2. Nickel-Aluminum-Bronze
3. Stainless Steel

Manganese bronze propellers are the most inexpensive to manufacture. Because of the ease with which it can be finished, manganese bronze has long been the traditional bronze propeller alloy. For the nickel-aluminum-bronze alloy, its high tensile strength allows the manufacturer to produce propellers with many built-in design features, such as thinner blade sections. The advantage of a thinner blade is less hydrodynamic drag which greatly improves a vessel's operating efficiency. This is the alloy that the U.S. Navy uses for naval vessels' propellers. Finally, propellers manufactured in stainless steels such as ASTM grade CF-3 austenitic stainless steel benefit from superior strength and damage resistance inherent in this extra low carbon stainless steel alloy.

Improved moulding processes such as centrifugal casting are used today in concurrent propeller hub manufactures, in cases where higher product quality and superior properties are needed. In centrifugal casting, the molten metal is poured into a hollow cylindrical mold spinning about either a horizontal or a vertical axis at speeds sufficient to develop 60 to 75 g (gravities) of centrifugal force [13]. This causes the liquid metal to flow to the outside of the mold and to remain there in the shape of a hollow cylinder. Heavier components within the metal are thrown outward with greater force than the lighter particles. This helps eliminate light nonmetallic particles and impurities, which are congregated inward toward the axis of rotation through flotation. These impurities can then be removed by a light machining operation.

Numerical control, as an application of automation of the fabrication process, is a complex control used to give physical movement, continuous or intermittent, through servomotors to the tool, machine table, or auxiliary functions. Table and tool movements can be made by electrical, hydraulic, or mechanical means, as long as the input signal represents a numerical value.

The two main types of numerical control are point-to-point positioning and continuous path control. In the case of propeller blade finishing, the continuous-path or contouring system is applied. This is by far the most complicated system of numerical control. In milling a profile of a three-dimensional surface, the entire path must be specified by the data input medium. The tool path can be of any shape, but the controls are such that the tool can move only in a straight line. The straight line distances may be as short as 0.0005 inches and so well blended that they will appear as a continuous smooth cut.

Blade finishing can be accomplished either by hand finishing or by NC machining. Hand finishing can be usually used for simpler blade designs and when tolerance requirements are less strict. NC machining is generally used when blade designs are more complicated, like in the case of highly skewed blades. In this case, stock

allowance on the blade pattern is of the order of 8 to 10 mm, whereas in the case of hand finishing it does not exceed 2 to 3 mm. For applications requiring meticulous precision and close tolerances, blades are NC machined to final dimensions on all hydrodynamics surfaces of the blade, including the pressure side suction side, leading edge, trailing edge, blade root and tip. No hand finishing is required in this case, except to remove tool marks. The following advantages are incorporated into NC machined blades:

1. Achievement of every design detail in the finished propeller.
2. Strict conformance with propeller design requirements in all areas.
3. High performance and quiet operation due to precise machining of the blade tip geometry as intended by the design.
4. Consistent repeatability, blade to blade. This way, only one in each set of four or five requires complete dimensional inspection.
5. Individual, precise balancing with no material removal or changes to hydrodynamic surfaces.
6. Capability of individual blade replacement while maintaining original balance tolerances of the entire propeller.

Leading companies in the production of propeller systems for ships currently offer full 5-axis contouring capability for bigger parts, or 3-axis contouring and conventional milling capability for smaller undertakings. As mentioned before, NC milling machines are used to finish propeller blades where extremely close tolerances are required. Contouring programs virtually for any project can nowadays be created through the use of state-of-the-art sophisticated CAD/CAM systems. Parts to be machined can be either programmed for the specific machining equipment by the manufacturer or NC data can be supplied by the customer.

5.2 Manufacturing Tolerances

Despite the advances in the propeller design and manufacturing science, tolerances have to be accepted, as it is impossible to make the product as it has originally

been designed. The level of confidence that can be attributed to the manufacturing process is directly proportional to the deviation from the design. Therefore, manufacturing tolerances should be included in the process to limit the effects on the confidence level to an insignificant amount, while at the same time being within the manufacturer's capabilities.

Two tolerance systems are widely used today for control of the propeller geometry. These are the ISO-R484-1981 [14] and the U.S. Navy system detailed by Standard Drawing 810-4435837 [15]. Both these tolerance systems are applicable to new propeller manufacture. Between the two systems, the Standard drawing is used for all U.S. Navy ship propeller procurements. As far as propeller repair tolerances, the U.S. Navy specifies repair tolerances similar to and based on the Standard Drawing, whereas for commercial applications no repair tolerances standard has been specified.

The purpose of both tolerance systems is to provide the design agency with a tolerance system that limits the allowable geometric variations and is accepted by the manufacturing industry, as well as to establish a certification procedure or minimum inspection requirements.

5.2.1 Tolerance Classes

Several tolerance classes have been established based on the possible variations and their effects on vessel performance, in concert with the manufacturing industry's capability.

The ISO tolerance system has four tolerance classes, based on manufacturing accuracy:

1. Class S: Very high tolerance
2. Class I: High accuracy
3. Class II: Medium accuracy

4. Class III: Wide tolerance

The correct tolerance class for a particular design has to be selected from the above classes by the design agency. The ISO does not provide guidance as to suitability of a particular manufacturing accuracy for a certain design.

As far as the U.S. Navy tolerance classes, only one accuracy class was until recently permitted as per [15] and [16]. Three accuracy classes or levels were later introduced by [17]:

1. Level 1: Strict tolerances
2. Level 2: Intermediate tolerances
3. Level 3: tolerances to suit the intended service

Among the U.S. Navy tolerance levels listed above, Level 1 tolerances are identical to the original Standard Drawing requirements. Level 2 permits a wider range in a few of the geometric variables, in particular the allowable gage clearance, which has to do with the inspection method implemented by this tolerance system. Level 3 does not list specific criteria, thus permitting the designer to choose the suitable tolerance method.

The analogous Military Specification for fixed pitch propellers lists also three tolerance levels based on the vessel's level of combat duty:

1. Combatant
2. Non-combatant
3. Service

Overall, it appears to be a qualitative correspondence between the two military specifications tolerance classes, implying that the tolerance level at least for the U.S. Navy is a function of the vessel's combat level [12].

Commercial or non-military propellers are almost exclusively manufactured, repaired, inspected, and certified according to the ISO 484 tolerance system. U.S. Navy

or military propellers on the other hand use the U.S. Navy tolerance system, whereas military propellers manufactured outside the U.S. are mostly constructed under the ISO 484. In summary, the ISO tolerances are generally much less restrictive than the U.S. Navy Standard Drawing. This has as a result less inspection data and geometric control, and less time and cost to certify. With the U.S. Navy gage method, the inspection procedure itself is much more detailed and thus much less ambiguous, which has certainly a negative impact in time and associated cost to certify.

5.3 Propeller Inspection

The ISO and U.S. Navy tolerance systems are associated with two distinctly different methods to verify that propeller blades are in compliance with specified tolerances [18].

The ISO system of tolerances is based on the use of a pitchometer. A pitchometer is a device for determining the propeller blade pitch angle by measuring the distance from a reference plane to points on the blade pressure face. In propeller inspection, key measurements are made on each blade at prescribed radii from the propeller axis. The pitchometer is used to locate the desired radii on the propeller blade surface. Having located the desired radii, the surface must be measured at prescribed points along each radius. These points are located using a custom template for the desired radius. For each one of the four manufacturing accuracy classes that are presented, ISO explicitly specifies tolerances on:

1. The pitch.
2. The extreme radius of the screw propeller.
3. The thickness of the blade section.
4. The form of the blade sections.
5. The length of the blade sections.
6. The location of blades, reference lines, and blade contours.
7. Rake, axial position and relative axial position of consecutive blades.

8. Surface finish.
9. Static balancing, and
10. Measuring equipment.

As mentioned before, propellers for merchant ships are almost exclusively manufactured and inspected using the pitchometer method.

The method required by the U.S. Navy to measure the accuracy of propeller blades is based upon the use of a series of sheet-metal template gages. Three types of sheet-metal template gages are used:

1. Suction and pressure face cylindrical contour gages.
2. Leading edge, trailing edge, and tip gages, and
3. Fillet and hub or palm gages.

Generally, a minimum of 53 gages is required to inspect a propeller.

The gage method provides considerably more insight and control over the blade geometry than does the pitchometer method; however, there is also an increase in cost. The cost increase is related to: the gages, which must be manufactured for each propeller design; the increased number of measurements, with more than 2.5 times as many required; the data gathering process, which is not easily automated; and the fact that the propeller is subject to errors because of the number of gages and measurements required. But, for applications where propeller accuracy is of critical importance, as is the case with some naval ships, such a rigorous measurement procedure is a necessity.

5.4 Advanced Propeller Inspection Methods

It is commonly accepted in the propeller manufacturing industry that using manual procedures such as pitchometers, templates and gages in the propeller measurement process is an extremely tedious, labor intensive and time-consuming task. As a result of an effort to improve the accuracy and repeatability and to lower the cost

associated with propeller manufacturing, recent manufacturing technology developments have led towards a more automated propeller measurement process.

5.4.1 Theodolite Systems

Precision theodolite systems provide the basis for numerous measurement applications in industrial metrology. Theodolite measuring systems are state-of-the art intelligent measuring systems which involve mechanical engineering, optics, electronics and software applications. Measuring more quickly and more precisely, as measurements are accomplished with considerably fewer manual settings and made faster, increases productivity. Thus, cost per production unit is minimized.

Theodolite measuring systems are used in the leading propeller manufacturing industry for collecting data, such as verifying propeller blades, checking their position and shape, and then comparing those with reference data. Because of their mobility and contactless measuring principle, they are ideal for using with very large objects, such as propellers and propeller blades, but also with delicate or inaccessible objects. Industrial measurement systems are based on optical precision instruments which by means of angle and distance measurements are able to deliver three-dimensional coordinates to a high degree of accuracy. The computed coordinates then provide the starting point for individual further processing operations, such as the determination of geometrical shape and position. Their flexibility in use and the accuracy and reliability of the measurement results, plus time saving operating processes make them extremely cost-effective in design, research, production and quality control operations.

Similarly to the manual procedure used in propeller inspection, propeller verification using a theodolite measuring system involves key measurements on each blade at prescribed radii from the propeller axis, at prescribed points along each radius. The measurement point is targeted with a telescope and a special reticule. The position of the object point at the angle of intersection between two or more theodilite sightings can then be determined to about 15 microns (15/1000 mm). This precision depends on the

setting accuracy and the automatic compensator which the system also comprises. Geometric verification process of machined variable pitch propeller blades involves one computer system, two theodolite heads, two operators, and two set-ups, one for each theodolite. The verification task is accomplished by measuring the propeller blade and then comparing the results to a CAD model.

5.4.2 Automated Propeller Optical Measurement System

The automated propeller optical measurement system (APOMS) is an earlier development towards automating the propeller inspection procedure. APOMS is intended to eliminate all of the drawbacks of the manual propeller measurement process by quickly and automatically producing detailed surface data via contactless three-dimensional optical sensing. Moreover, APOMS can measure an unfinished propeller casting, compare the shape with a CAD/CAM description of the machined propeller and verify that the casting has sufficient material for machining of the desired propeller [19].

APOMS consists of a three-dimensional noncontacting optical sensor system, a custom designed precision 5-axis robot and a minicomputer. The optical sensor system is a contactless coordinate measuring device which automatically provides precise unambiguous three-dimensional surface measurement data in real time. The vision sensor operates on the principle of optical triangulation between a projected structured light pattern and the location of its image on the surface as sensed by an offset camera. The vision processor is capable of real time data processing, which allows the minicomputer to perform data analysis computations in almost real time.

Again, propeller blade inspection is performed at a set of radial distances from the central axis of the hub and involves comparison of design and measured surface data and analysis of their discrepancies. APOMS can measure both blade and hub surfaces of a large propeller in approximately 10 hours, as well as duplicate the manual measurement procedure in approximately 2 hours.

In a further development towards the automation of propeller manufacture, APOMS can be integrated and cooperate with two other systems, the propeller robotic automated templating system (PRATS), and the propeller robotic finishing system (PROFS). These systems automate the finishing of propeller castings to produce finished propellers. PRATS compares the measurement data produced by APOMS with the propeller design data and optimizes the placement and orientation of the finished propeller surface within the envelope defined by the unfinished propeller casting. In its turn, PROFS computer calculates the amount of material to be removed from the unfinished propeller, by using visual information obtained via a vision sensor. Then, the robot can precisely grind the propeller casting until the desired finished surface is obtained.

Chapter 6

6 Economic Impact of Propeller Manufacturing Tolerances

6.1 Background

This chapter examines the economic impact of manufacturing a propeller according to certain tolerance system specifications and the associated savings in ship's operating cost. The propeller considered for the economic analysis is the U.S. Navy DDG-51 destroyers' class propeller, manufactured according to the U.S. Navy Standard Drawing tolerance system.

The issue of the selection of the appropriate tolerance system for a propeller manufacture is analyzed in [12]. This paper introduces a rational approach for establishing manufacturing tolerances for propellers by quantifying the sensitivity of certain propeller performance characteristics to dimensional variations in blade geometry allowed by the various tolerance systems and classes. According to this study, four

different performance characteristics that have a direct impact on ship operability are examined:

1. Ship Speed, V_S
2. Propeller RPM, n
3. Quasi-Propulsive efficiency, QPC
4. Cavitation number margin on back bubble cavitation, σ_M

According to [12], these performance characteristics mentioned above are considered to be the dependent variables, each one of them is considered to be a function of a set of blade geometric characteristics which are the independent variables. A tolerance system establishes the maximum allowable variation in these geometric characteristics. This way, the variation in each performance characteristic because of the variation in each one of the propeller geometric characteristics can be determined for a given propeller design. Three obvious geometric characteristics are then selected for the study, for the reason that their variations are expected to influence the selected performance characteristics significantly. These are:

1. Blade pitch, P
2. Blade camber, f_0, and
3. Blade thickness t_0

This chapter examines the economic impact of manufacturing a propeller according to a certain tolerance system/class. The two tolerance systems, ISO classes S, I and II, and U.S. Navy are examined. The economic impact is examined in terms of the percent reduction in QPC that corresponds to the percent variation in each one of the previously mentioned geometric characteristics allowed by each tolerance system/class. These "effective" tolerances, adjusted accordingly from the actual ones to capture the ambiguity and inaccuracy of the systems, refer to new propeller manufacture and are shown in Table 6-1.

Table 6-1. Effective Tolerances in Propeller Geometric Characteristics.

	ΔP (%)	Δf_0 (%)	Δt_0 (%)
U.S. Navy Standard Drawing	±1.25	±2.5	+1 -3
ISO Class S	±1.5	±10	+3 -2
ISO Class I	±2.0	±15	+3.5 -2.5
ISO Class II	±3.0	±25	+5 -3

Based on the analysis performed in [12], these tolerances in each one of the considered propeller geometric characteristics affect the propeller performance. In addition, there is also a variation in manufacturing cost associated with the tolerance system that propeller manufacture complies with. By using the ISO Class I system as the baseline, [12] estimates the percent increase or decrease in manufacturing cost by complying with any of the other tolerance systems considered. Table 6-2 shows the resulting allowable reduction in QPC and the percent difference in manufacturing cost associated with the four tolerance systems/classes considered.

Table 6-2. Allowable Reduction in QPC and Relative Difference in Manufacturing Cost.

	U.S. Navy Standard Drawing	ISO Class S	ISO Class I	ISO Class II
ΔQPC (%)	1.4	2.5	4.1	6.7
Δc (%)	+31	+15	0	-10

The percentages shown in table 6-2 refer to the case examined by the study, which is the propeller for a Matson Lines container ship. Because of the analogies in gross propeller characteristics between the case propeller and the one of the DDG-51 class, it was assumed that these values can be applied to the case examined in this chapter without significant error.

6.2 Assumptions

The principal characteristics of the DDG-51 destroyer class propeller that is used for this analysis are shown in Table 6-3. In addition, Table 6-4 shows the propeller

characteristics for the two steaming conditions examined in this analysis, endurance and sustained.

Table 6-3. Characteristics of DDG-51 Propeller.

Propeller Model	4988
Number of Shafts	2
Propeller Diameter (ft)	17.0
Number of Blades	5
Pitch Ratio	1.72
Expanded Area Ratio	0.784
Thrust Deduction Coefficient	0.055
Taylor Wake Fraction	0.020
Hull Efficiency	0.964
Relative Rotative Efficiency	0.985
Total Propeller Weight (lton)	51.62

Table 6-4. Endurance and Sustained Condition Characteristics.

	Conditions	
Characteristics	**Sustained**	**Endurance**
Speed (knots)	29.63	20.00
RPM	149.8	91.8
Thrust/Shaft (lbf)	312,626	94,332
EHP/Shaft (hp)	26,866	5,471
Torque/Shaft (ft.lbf)	1,385,327	436,585
SHP/Shaft (hp)	40,124	7,746
Advance Coefficient (J)	1.155	1.272
Thrust Coefficient (KT)	0.302	0.242
Torque Coefficient (10KQ)	0.786	0.660
Open Water Efficiency	0.705	0.744
Propulsive Coefficient	0.670	0.706

A total number of 150 days per year underway was assumed. Because of the dramatic increase in effective horsepower, EHP, from the ship's endurance to sustained condition, an operating profile of 90 percent of this time underway was assumed to be under endurance speed, while the rest 10 percent was taken to be in sustained speed. Also, a total number of 28 ships was assumed for the class. Other leading assumptions that this analysis is based on are:

- By assuming the propulsion plant consists of GE LM2500-30 gasturbines, the specific fuel consumption, sfc, was taken to be 0.3929 lb/(hp.hr).
- EHP_E and EHP_S, the effective horsepower in endurance and sustained condition respectively, were in total taken to be 10,942 and 53,732 hp respectively.
- By adopting the operating profile previously discussed for the DDG-51 for a total number of 3600 hours, which corresponds to 150 days at sea per year, the total number of hours at sea in endurance condition, HAS_E is equal to 3240 hours and in sustained condition, HAS_S 360 hours.
- The fuel oil price, FP, was assumed to be 0.95 $/gal.
- Fuel oil density, d, is taken to be 6.8 lb/gal.
- The total number of ships N_S for the DDG-51 program is 28.
- The base year for the cost analysis was 2001.
- All the DDG-51 class ships were assumed to have 30 years of useful life.
- The discount rate for the life cycle savings due to fuel savings was assumed to be 10 percent.
- To simplify the analysis, all the ships were assumed to start out their useful life simultaneously at the base year, i.e., no production rate was taken in to account.

6.3 *Life Cycle Savings by Complying with the U.S. Navy Standard Drawing Tolerance System*

Based on the general definition of the efficiency of an engineering operation, the propulsive coefficient, PC, is the ratio of the effective horsepower, EHP, which is the

useful power to overcome the resistance of a ship to move at a certain speed, to the shaft horsepower, SHP, which is the power delivered to the shafting abaft the gearing:

$$PC = \frac{EHP}{SHP} \tag{6-1}$$

The quasi-propulsive efficiency, QPC, is a more meaningful measure of efficiency of propulsion since it does not take into account mechanical efficiencies, gear losses and shaft transmission losses which all vary from ship to ship [21]. Hence, the QPC is defined to be the ratio of the effective horsepower, EHP, to the delivered horsepower, DHP, which is the power actually delivered to the propeller:

$$QPC = \frac{EHP}{DHP} \tag{6-2}$$

QPC and PC are related through hull efficiency, n_H, the ratio of DHP to SHP:

$$n_H = \frac{DHP}{SHP} \tag{6-3}$$

Hence, QPC is the product of PC by n_H:

$$QPC = PC \cdot n_H \text{, or equivalently, } PC = \frac{QPC}{n_H} \tag{6-4}$$

Therefore, tolerance changes in QPC can be directly associated with identical changes in PC, since n_H is constant and equal to 0.964 in the DDG-51 case.

The following formula was used for the assessment of the annual fuel consumption cost, AFC:

$$AFC = \frac{sfc \cdot (\frac{EHP_E}{PC_E} \cdot HAS_E + \frac{EHP_S}{PC_S} \cdot HAS_S) \cdot FP}{d} \cdot N_S \tag{6-5}$$

where, sfc is the specific fuel consumption in lb/(hp.hr), HAS is the number of hours at sea per year, FP is the fuel oil price in $/gal, and d is the fuel oil density in lb/gal. The indices E and S refer to the endurance and sustained steaming conditions respectively.

Based on the values shown in Table 6-2 for the resulting allowable reduction in QPC per tolerance class, a relative QPC reduction factor was established between tolerance classes. This reduction factor was used to determine the endurance and sustained propulsive coefficients at which the analysis was performed. The relative reduction factor was estimated as follows:

1. $\Delta QPC_{ISO\_S} - \Delta QPC_{S\tan dard\_Drawing} = 0.011$
2. $\Delta QPC_{ISO\_I} - \Delta QPC_{S\tan dard\_Drawing} = 0.027$
3. $\Delta QPC_{ISO\_II} - \Delta QPC_{S\tan dard\_Drawing} = 0.053$

Table 6-5 lists the endurance and sustained propulsive coefficient values that were used in the analysis. These values were derived by subtracting the previously calculated reduction factors from the actual DDG-51 values shown in Table 6-4. DDG-51 values are the baseline since DDG-51 propellers are manufactured according to U.S. Standard Drawing tolerance specifications.

Table 6-5. Endurance and Sustained Propulsive Coefficients.

	PC_E	PC_S
U.S. Navy Standard Drawing	0.706	0.670
ISO Class S	0.695	0.659
ISO Class I	0.679	0.643
ISO Class II	0.653	0.617

By using the annual fuel cost calculated for the U.S. Navy Standard Drawing propulsive coefficients as the baseline cost, the annual fuel savings resulting from using the U.S. Navy standard drawing tolerance system versus each one of the ISO tolerance classes were calculated. The following formula provides the annual fuel savings:

$$AS = AFC_i - AFC_0 \tag{6-6}$$

where, AFC_i the annual fuel cost for each one of the ISO tolerance classes and AFC_0 the annual fuel cost for the U.S. Navy Standard Drawing tolerance system. The present value of the total fuel savings, for a 30-year useful life of the class was estimated as follows:

$$PV(AS) = AS \cdot \sum_{t=1}^{30} \frac{1}{(1+i)^t} \tag{6-7}$$

where i the discount rate.

Table 6-6 lists the input parameters that were used in the analysis and Table 6-7 summarizes the results of aforementioned calculations. Calculations are shown in Appendix I.

Table 6-6. Input Parameters.

EHP_E	10,942
EHP_S	53,732
Hours at sea per year, endurance speed	3,240
Hours at sea per year, sustained speed	360
Specific fuel consumption (lb/(hp.hr))	0.3929
Fuel price ($/gal)	0.95
Fuel density (lb/gal)	6.8
Total number of ships in class	28
Ship's useful life (years)	30
Discount rate (%)	10

Table 6-7. Fuel savings calculations for the various tolerance systems.

	U.S. Navy Standard Drawing	ISO Class S	ISO Class I	ISO Class II
PC_E	0.706	0.695	0.679	0.653
PC_S	0.670	0.659	0.643	0.617
Annual Fuel Cost ($M)	121.5	123.5	126.5	131.6
Annual Fuel Savings ($M)	-	(2.0)	(4.9)	(10.0)
PV of Fuel Savings ($M)	-	(18.5)	(46.5)	(95.0)

By examining the results of Table 6-7, the benefits of complying with the specific tolerance system for propeller manufacture, at least from an annual savings point of view, are obvious. For the particular case of the DDG-51 that is examined here, it might not make much sense to compare the resulting savings against the ISO classes I and II, as both these classes are probably far from meeting the strict U.S. Navy performance criteria. However, ISO class S specifications are quite close to the U.S. Navy's and a comparison between those two classes is legitimate.

As can be seen from Table 6-7, complying with the U.S. Navy Standard Drawing versus the ISO Class S results in an annual saving of $2 million. Although this number only represents a small percentage of the total annual operating cost of the DDG-51 class, it is significant because of the fact that it is due to a very small reduction of 1.1 percent in propulsive coefficient between the two tolerance classes. Moreover, for the whole lifespan of the class, these savings rise as high as $18.5 million.

Table 6-8 shows the impact that the use of a different discount rate has on the present value calculations. As is expected, lifetime savings become of considerably more importance if lower discount rates are used.

Table 6-8. Cost of capital sensitivity analysis.

Cost of capital sensitivity analysis	U.S. Navy Standard Drawing	ISO Class S	ISO Class I	ISO Class II
Annual Fuel Savings ($M)	-	(2.0)	(4.9)	(10.0)
Vessel's economic life (years)	30	30	30	30
PV of fuel savings ($M) (i=5.0%)	-	(30.2)	(75.8)	(154.9)
PV of fuel savings ($M) (i=7.5%)	-	(23.2)	(58.3)	(119.0)
PV of fuel savings ($M) (i=10.0%)	-	(18.5)	(46.5)	(95.0)
PV of fuel savings ($M) (i=12.5%)	-	(15.2)	(38.3)	(78.3)
PV of fuel savings ($M) (i=15.0%)	-	(12.9)	(32.4)	(66.2)
PV of fuel savings ($M) (i=17.5%)	-	(11.1)	(28.0)	(57.1)
PV of fuel savings ($M) (i=20.0%)	-	(9.8)	(24.6)	(50.2)

6.4 Sensitivity Analysis Results

There is no doubt that the U.S. Navy Standard Drawing tolerance system is used in most U.S. Navy propellers manufacture because it meets certain strict performance criteria for naval vessels. In order to assess the usefulness of complying with the U.S. Navy Standard Drawing tolerance system for the DDG-51 class propellers, from an economics point of view, it is important to estimate the effects of tolerance changes on propeller manufacturing costs. A tolerance change will affect all the series of the propeller manufacturing events shown in Figure 5-1, with the exception of hub/palm machining. In particular, blade finishing and certification costs are going to be the two costs affected the most.

Table 6-2 shows that the cost to manufacture a propeller according to the U.S. Navy Standard Drawing specifications is 31 percent higher than the cost of manufacture

according to ISO Class I. Also, the cost to manufacture to ISO Class S is 15 percent higher than to ISO Class I. Therefore, the cost to manufacture to U.S. Navy Standard Drawing is approximately 14 percent higher than the cost to ISO Class S. By following a trial-and-error procedure, we can find that the break-even cost for a propeller for the DDG-51 class, manufactured to U.S. Navy Standard Drawing, is approximately $2.7 million. This means that an identical propeller manufactured to ISO Class S would cost around $2.36 million and eventually, for the total number of propellers of the DDG-51 class, the difference in manufacturing cost would offset the present value of savings of $18.5 million in fuel cost, associated with the use of the U.S. Navy Standard Drawing propellers. For a cost less than $2.7 million per propeller, the break-even cost, complying with the stricter U.S. Navy standards results in a positive Net Present Value and makes the U.S. Navy Standard Drawing propellers more desirable, even from an economical point of view.

By using a costing method which is based on Cost Estimating Ratios (CERs), an initial cost estimate for the DDG-51 propeller was achieved. Using CERs for both labor cost, in terms of hr/lton, and material cost, in terms of $/lton, and by multiplying labor cost with wage in terms of $/hr, the estimate for the DDG-51 cost was of the order of $1.4 million. This number was also confirmed to reflect the reality after consultation with experts in the propeller manufacturing industry. With cost being at this magnitude and following the previous discussion, complying with the U.S. Navy Standard Drawing tolerance system for the DDG-51 case seems to be desirable from a Net Present Value point of view.

Chapter 7

7 Conclusions

A new algorithm for blade shape alignment in *PBD-14* design mode is investigated in this study. The need for this new approach in blade shape manipulation is generated from the effort to overcome the drawbacks associated with the existing blade shape adjustment scheme in *PBD-14*. The new algorithm requires the blade mean camber surface to exactly match the streamlines of the local flow field in which the blade operates, so that the blade will be tangent to the local flow as dictated by the blade design process. A quick review of the steps followed by the new design approach is included:

1. Starting from a "generator line" which is formed by a set of vortex/source lattice nodes in the spanwise direction, characterized by the same chordwise number N, the total velocity at each one of these nodes is evaluated.
2. Using the total velocity information at the set of nodes mentioned above, the streamlines of the local flow field in which the blade operates are traced and the next spanwise set of nodes in the chordwise direction is placed on those streamlines.

3. Repeating the previous two steps for all the spanwise sets of nodes, the blade mean camber surface is fitted so that it matches the streamlines of the local flow field in which the blade operates.
4. The new, perturbed blade mean camber surface is finally fitted with a B-spline surface.

Three design example cases were used to validate the new blade design algorithm. These include a single open propeller stand-alone design, the same single open propeller design case this time coupled with a flow solver, and, a water jet design coupled with a flow solver.

Results from all three design cases confirm the robustness of the new design algorithm. In all cases, the resulting blade shape was free of spanwise corrugations, which were the major concern in most of the cases with the existing design algorithm. Moreover, the output blade shape in all the test cases presents smooth and fair characteristics. This is particularly important from a manufacturing point of view, as a blade with poor fairness characteristics may not be easily manufactured. Finally, the output blade from all design cases recovers the design circulation quite well. Further testing is needed though, in order to justify some discrepancies between the design and the solved circulation distribution, as is the case with the second design example.

Another benefit that the new blade shape alignment algorithm has is its "one step" design capability. That means that there are not internal blade shape iterations, as was the case with the existing design algorithm. Instead, the design process leads to the final output in one *PBD-14* run. Like the existing scheme, more runs are certainly needed for convergence, especially if the final blade represents a big departure from the initial blade. Overall, the "one-step" methods is found to aid convergence, which in general occurs faster than with the existing design algorithm. A drawback of the new scheme however is that it generally slows down the design process, in particular when very fine blade discretization is used. Fine blade discretization is essential for the accuracy of the

process, as discussed in Chapter 3. The penalty though is that the process becomes more memory intensive and, as a result, slower.

This study also examines the propeller from a manufacturing point of view, focusing on propeller inspection and verification issues, based on specific manufacturing tolerances. In particular, it briefly overviews the propeller manufacturing procedure, presenting new technologies and current trends in the sequence of the events that constitute the propeller manufacture. It discusses the various manufacturing tolerance systems and classes, as well as their major characteristics and differences. Finally, it presents the major propeller inspection methods, both traditional and new, as well as their benefits and shortcomings.

A cost analysis of the impact of propeller manufacturing tolerances on a ship's operating cost is performed. The analysis is performed using the U.S. Navy DDG-51 destroyers' class propeller, manufactured according to the U.S. Navy Standard Drawing tolerance system, as an example propeller. Based on the assumptions that it was performed, the analysis revealed that, for the specific class of ships, the resulting fuel savings over the ship's class life due to the increased propulsive efficiency more than offset the considerably increased manufacturing cost associated with the specific propeller manufacture according to the U.S. Navy Standard Drawing tolerance system. Moreover, this difference may become even more significant in the future as fuel price follows an increasing trend and, on the other hand, the increasing use of modern, automated propeller verification methods by the industry is expected to reduce propeller manufacturing cost considerably.

The cost analysis performed in the last part of this thesis was based on the assumptions stated in the beginning of Chapter 6. Several of these assumptions, such as the relative differences in propulsive efficiencies and manufacturing costs between the various tolerance classes are based on a qualitatively similar propeller rather than the one actually used in this analysis, because of lack of actual data. However, trends are expected to be similar and not deviate significantly if actual data for the example

propeller was used in all cases. In addition, fuel price plays the most important role in the life cycle fuel savings calculation and may need to be modified to reflect future trends. Hence, further investigation is needed for the adjustment of the assumptions used.

Bibliography

[1] J. E. Kerwin. A Vortex Lattice Method for Propeller Blade Design: MIT-PBD-10 User's Manual. Technical Report 84-2, MIT Department of Ocean Engineering, January 1984.

[2] L. Leibman and J. E. Kerwin. An enhanced vortex lattice propeller design method: MIT-PBD-10.1 user's manual. Technical report, MIT Department of Ocean Engineering, January 1991.

[3] D. S. Greely and J. E. Kerwin. Numarical Methods for Propeller Design and Analysis in Steady Flow. *SNAME Transactions*, 90, 1982

[4] J. E. Kerwin, S. D. Black, T. E. Taylor, and C. L. Warren. A Design Procedure for Marine Vehicles with Integrated Propulsors. In *Propellers/Shafting '97 Symposium*, Virginia Beach, VA, September 1997. Ships' Machinery Committee, SNAME.

[5] J. E. Kerwin, T. E. Taylor, S. D. Black, and G. McHugh. A Coupled Lifting-Surface Analysis Technique for Marine Propulsors in Steady Flow. In *Propellers/Shafting '97 Symposium*, Virginia Beach, VA, September 1997. Ships' Machinery Committee, SNAME.

[6] T. E. Taylor, J. Otto Scherer, and J. E. Kerwin. Waterjet Pump Design and Analysis Using a Coupled Lifting-Surface and RANS Procedure. In *Royal Institution of Naval Architects Conference on Waterjet Propulsion – Latest Developments*, Amsterdam, The Netherlands, 1998.

[7] C-Y Hsin. User's manual for MIT-PSF-10.10. Technical Report, MIT Department of Ocean Engineering, January 1990.

[8] J. E. Kerwin, D. P. Keenan, S. D. Black, and J. G. Diggs. A Coupled Viscous/Potential Flow Design Method for Wake-Adapted, Multi-stage, Ducted Propulsors. In *Proceedings, Society of Naval Architects and Marine Engineers*, 1994.

[9] N. J. Hahn, A. M. Polsenberg, D. H. Renick, T. E. Taylor, and J. E. Kerwin. PBD-14.3: A Coupled Lifting-Surface Design/Analysis Program for Marine Propulsors. Technical Report, MIT Department of Ocean Engineering, April 5, 2000.

[10] B. Smith, G. R. Rinaudot, K. A. Reed, and T. Wright. Initial Graphics Exchange Specification (IGES), Version 4.0. Technical Report NBSIR 88-3813, National Bureau of Standards, 1988.

[11] B. M. Ayyub, R. H. McCuen. Numerical Methods for Engineers. Prentice-Hall, Inc., 1996.

[12] G. V. Cole, W. S. Vorus, and R. F. Kress. A Rational Approach to Propeller Manufacturing Tolerances. In *Proceedings, Propellers '84 Symposium*, SNAME, 1984.

[13] R. A. Lindberg. Materials and Manufacturing Technology. Allyn and Bacon, Inc., August 1979.

[14] Shipbuilding, Ship Screw Propellers, Manufacturing Tolerances Part I: Propellers of Diameter Greater than 2.5 Meters. International Standard (ISO) R484/1981.

[15] Propeller. NAVSHIPS Standard Drawing 810-4435837, Department of the Navy, January 1969.

[16] Propeller Blade Gauge design and Application. NAVSEA Technical Manual 0987-LP-011-2000.

[17] Propellers, Ship, Controllable Pitch. MILSPEC DOD-P-24562 (SH), December 1977.

[18] Marine Engineering. The Society of Naval Architects and Marine Engineers, 1992.

[19] H. K. Stern, R. J. Metzger. Automation of Propeller Inspection and Finishing. Naval Engineers Journal vol. 97, May 1985. ASNE Day 1985 Technical Paper. Washington, DC, 1985.

[20] Instructions for Design of Marine Propeller Blade Gages. Technical Manual, NAVSEAbS9245-AP-TSM-010/PROP. Department of the Navy.

[21] Principles of Naval Architecture. Second Revision. The Society of Naval Architects and Marine Engineers, 1988.

[22] S. Denny. Cavitation and Open Water Performance Tests of a Series of Propellers Designed by Lifting-Surface Methods. Technical Report 2878, DTNSRDC, 1968.

[23] Stuart D. Jessup. *An Experimental Investigation of Viscous Aspects of Propeller Blade Flow*. PhD thesis, The Catholic University of America, June 1989.

[24] T. E. Taylor. *Preliminary Design and Analysis of Propulsors for Axisymmetric Underwater Vehicles*. PhD thesis, MIT Department of Ocean Engineering, September 1996.

[25] A.M. Polsenberg, J. E. Kerwin and T.E. Taylor. A Manual for the Coupling of PBD-14 and DTNSAX: A Coupled Lifting-Surface Design/Analysis Program for Marine Propulsors. Technical Report, MIT Department of Ocean Engineering, April 5, 2000.

Appendix I: Fuel Savings Calculation

Fuel savings calculation

Definition of units:

$dol := coul$

$Mdol := 10^6 \cdot dol$

Definition of variables:

Specific fuel consumption: $sfc := 0.3929 \frac{lb}{hp \cdot hr}$

Total number of ships for the DDG-51 class: $N_S := 28$

Fuel oil price: $FP := 0.95 \frac{dol}{gal}$

Fuel oil density: $d := 6.8 \frac{lb}{gal}$

Effective horsepower, endurance condition: $EHP_E := 10942\,hp$

Effective horsepower, sustained condition: $EHP_S := 53732\,hp$

Hours at sea per year, endurance condition: $HAS_E := 3240\,hr$

Hours at sea per year, sustained condition: $HAS_S := 360\,hr$

$i := 0, 1 .. 3$

Propulsive coefficients, endurance condition: $PC_{E_i} :=$

0.706	U.S. Navy Standard Drawing
0.695	ISO Class S
0.679	ISO Class I
0.653	ISO Class II

Propulsive coefficients, sustained condition: $PC_{S_i} :=$

0.670	U.S. Navy Standard Drawing
0.659	ISO Class S
0.643	ISO Class I
0.617	ISO Class II

Annual fuel cost:

$$AFC := N_S \frac{sfc \cdot \left(\frac{EHP_E}{PC_E} \cdot HAS_E + \frac{EHP_S}{PC_S} \cdot HAS_S \right) \cdot FP}{d} \qquad AFC = \begin{pmatrix} 121.55 \\ 123.513 \\ 126.483 \\ 131.626 \end{pmatrix} \text{Mdol}$$

Annual fuel savings:

$$AS := AFC_0 - AFC \qquad AS = \begin{pmatrix} 0 \\ -1.962 \\ -4.932 \\ -10.076 \end{pmatrix} \text{Mdol}$$

Ship's useful life: 30 years

Discount rate range:

$$j := 0.05, 0.075 .. 0.2$$

Present value of fuel cost:

$$PVC(j) := AFC \cdot \sum_{t=1}^{30} \left[\frac{1}{(1+j)^t} \right]$$

Present value of fuel savings:

$$PVS(j) := AS \cdot \sum_{t=1}^{30} \left[\frac{1}{(1+j)^t} \right]$$

Present value of fuel savings, discount rate 5%:

$$PVS(0.05) = \begin{pmatrix} 0 \\ -30.164 \\ -75.819 \\ -154.887 \end{pmatrix} \text{Mdol}$$

Present value of fuel savings, discount rate 7.5%:

$$PVS(0.075) = \begin{pmatrix} 0 \\ -23.174 \\ -58.251 \\ -118.997 \end{pmatrix} \text{Mdol}$$

Present value of fuel savings, discount rate 10%:

$$PVS(0.10) = \begin{pmatrix} 0 \\ -18.497 \\ -46.495 \\ -94.982 \end{pmatrix} \text{Mdol}$$

Present value of fuel savings, discount rate 12.5%:

$$PVS(0.125) = \begin{pmatrix} 0 \\ -15.239 \\ -38.305 \\ -78.251 \end{pmatrix} \text{Mdol}$$

Present value of fuel savings, discount rate 15%:

$$PVS(0.15) = \begin{pmatrix} 0 \\ -12.884 \\ -32.384 \\ -66.156 \end{pmatrix} \text{Mdol}$$

Present value of fuel savings, discount rate 17.5%:

$$PVS(0.175) = \begin{pmatrix} 0 \\ -11.124 \\ -27.96 \\ -57.119 \end{pmatrix} \text{Mdol}$$

Present value of fuel savings, discount rate 20%:

$$PVS(0.20) = \begin{pmatrix} 0 \\ -9.77 \\ -24.557 \\ -50.166 \end{pmatrix} \text{Mdol}$$

Break-even cost calculation:

Cost of propeller manufacture according to U.S. Navy Standard Drawing (for the total number of ships of the class): C_{SD}

Cost of propeller manufacture according to U.S. Navy Standard Drawing (for a single propeller): C_{sd}

Cost of propeller manufacture according to ISO Class S (for the total number of ships of the class): C_S

Cost of propeller manufacture according to ISO Class S (for a single propeller): C_s

For a discount rate of 10%, the difference between the present values of the fuel savings with the two class systems is:

$$Diff := PVS(0.1)_0 - PVS(0.1)_1 \qquad Diff = 18.497\text{Mdol}$$

Since C_{SD}=1.14*C_S, by setting C_{SD}-C_S=Diff we take: $C_S := \frac{Diff}{0.14}$

Hence, the break-even cost for an ISO Class S propeller is given by:

$$C_s := \frac{C_S}{2 \cdot N_S} \qquad C_s = 2.359\text{Mdol}$$

Also, for a U.S. Navy Standard Drawing propeller, the break-even cost is:

$$C_{sd} := 1.14 C_s \qquad C_{sd} = 2.69\text{Mdol}$$